



Publication Year	2024
Acceptance in OA	2025-03-28T14:21:32Z
Title	Fundamental physics measurements with Galileo FOC satellites and the Galileo for science project. I. A 3D-CAD and a box wing for modeling the effects of nonconservative forces
Authors	LUCCHESI, David, VISCO, Massimo, LEFEVRE, CARLO, LUCENTE, Marco, SANTOLI, Francesco, SAPIO, Feliciano, CINELLI, MARCO, DI MARCO, Alessandro, FIORENZA, Emiliano, LOFFREDO, Pasqualino, MAGNAFICO, Carmelo, PERON, ROBERTO, Vespe, Francesco
Publisher's version (DOI)	10.1103/PhysRevD.109.062004
Handle	http://hdl.handle.net/20.500.12386/36977
Journal	PHYSICAL REVIEW D
Volume	109

Journal: Physical Review D
Accession code: DG13637
Article Title: Fundamental physics measurements with Galileo FOC satellites and the Galileo for science project. I. A 3D-CAD and a box wing for modeling the effects of nonconservative forces
First Author: David Lucchesi

AUTHOR QUERIES - TO BE ANSWERED BY THE CORRESPONDING AUTHOR:

The numbered items below correspond to numbers in the margin of the proof pages pinpointing the source of the question and/or comment. The numbers will be removed from the margins prior to publication.

Q: Please check that all references include complete titles.

Q1	Fifth Proof: Please check and verify closely to confirm all of the corrections have been incorporated properly throughout this Paper and also approve the Paper is ready to be published in its current form.
----	---

Important Notice to Authors

No further publication processing will occur until we receive your response to this proof.

Attached is a PDF proof of your forthcoming article in *Physical Review D*. The article accession code is DG13637.

Please note that as part of the production process, APS converts all articles, regardless of their original source, into standardized XML that in turn is used to create the PDF and online versions of the article as well as to populate third-party systems such as Portico, Crossref, and Web of Science. We share our authors' high expectations for the fidelity of the conversion into XML and for the accuracy and appearance of the final, formatted PDF. This process works exceptionally well for the vast majority of articles; however, please check carefully all key elements of your PDF proof, particularly any equations or tables.


Figures submitted electronically as separate files containing color appear in color in the online journal.

However, all figures will appear as grayscale images in the print journal unless the color figure charges have been paid in advance, in accordance with our policy for color in print (<https://journals.aps.org/authors/color-figures-print>).

Titles in References

The editors now encourage insertion of article titles in references to journal articles and e-prints. This format is optional, but if chosen, authors should provide titles for *all* eligible references. If article titles remain missing from eligible references, the production team will remove the existing titles at final proof stage.

ORCIDs

Please follow any ORCID links () after the authors' names and verify that they point to the appropriate record for each author. Requests to add ORCIDs should be sent no later than the first proof revisions. If authors do not subsequently add/authenticate ORCIDs within seven business days, production of the paper will proceed and no further requests to add ORCIDs will be processed. See complete details regarding ORCID requests and ORCID verification at <https://journals.aps.org/authors/adding-orcids-during-proof-corrections>. If this paper is an Erratum or a Reply, the corresponding author's ORCID may be present if previously provided to APS, but no ORCIDs can be added at proof stage.

Crossref Funder Registry ID:

Information about an article's funding sources is now submitted to Crossref to help you comply with current or future funding agency mandates. Crossref's Funder Registry (<https://www.crossref.org/services/funder-registry/>) is the definitive registry of funding agencies. Please ensure that your acknowledgments include all sources of funding for your article following any requirements of your funding sources. Where possible, please include grant and award ids. Please carefully check the following funder information we have already extracted from your article and ensure its accuracy and completeness:

- Agenzia Spaziale Italiana, FundRef ID <http://dx.doi.org/10.13039/501100003981> (IT/Repubblica Italiana)

Other Items to Check

- Please note that the original manuscript has been converted to XML prior to the creation of the PDF proof, as described above. Please carefully check all key elements of the paper, particularly the equations and tabular data.
- Title: Please check; be mindful that the title may have been changed during the peer-review process.
- Author list: Please make sure all authors are presented, in the appropriate order, and that all names are spelled correctly.
- Please make sure you have inserted a byline footnote containing the email address for the corresponding author, if desired. Please note that this is not inserted automatically by this journal.
- Affiliations: Please check to be sure the institution names are spelled correctly and attributed to the appropriate author(s).

- Receipt date: Please confirm accuracy.
- Acknowledgments: Please be sure to appropriately acknowledge all funding sources.
- References: Please check to ensure that titles are given as appropriate.
- Hyphenation: Please note hyphens may have been inserted in word pairs that function as adjectives when they occur before a noun, as in “x-ray diffraction,” “4-mm-long gas cell,” and “*R*-matrix theory.” However, hyphens are deleted from word pairs when they are not used as adjectives before nouns, as in “emission by x rays,” “was 4 mm in length,” and “the *R* matrix is tested.”
Note also that Physical Review follows U.S. English guidelines in that hyphens are not used after prefixes or before suffixes: superresolution, quasiequilibrium, nanoprecipitates, resonancelike, clockwise.
- Please check that your figures are accurate and sized properly. Make sure all labeling is sufficiently legible. Figure quality in this proof is representative of the quality to be used in the online journal. To achieve manageable file size for online delivery, some compression and downsampling of figures may have occurred. Fine details may have become somewhat fuzzy, especially in color figures. The print journal uses files of higher resolution and therefore details may be sharper in print. Figures to be published in color online will appear in color on these proofs if viewed on a color monitor or printed on a color printer.
- Overall, please proofread the entire *formatted* article very carefully. The redlined PDF should be used as a guide to see changes that were made during copyediting. However, note that some changes to math and/or layout may not be indicated.

Ways to Respond

- **Web:** If you accessed this proof online, follow the instructions on the web page to submit corrections.
- **Email:** Send corrections to aps-robot@luminad.com. Include the accession code DG13637 in the subject line.

If You Need to Call Us

You may leave a voicemail message at +1.855.808.3897. Please reference the accession code and the first author of your article in your voicemail message. We will respond to you via email.

1
2
3
4
5
6
7
8
9
10
11
12
13
14
15
16

Fundamental physics measurements with Galileo FOC satellites and the Galileo for science project. I. A 3D-CAD and a box wing for modeling the effects of nonconservative forces

David Lucchesi^{1,2,3,*}, Massimo Visco^{1,2}, Carlo Lefevre¹, Marco Lucente¹, Francesco Santoli¹,
Feliciano Sapio^{1,4}, Marco Cinelli¹, Alessandro Di Marco¹, Emiliano Fiorenza¹, Pasqualino Loffredo¹,
Carmelo Magnafico¹, Roberto Peron¹ and Francesco Vespe⁵

¹*Istituto Nazionale di Astrofisica (INAF), Istituto di Astrofisica e Planetologia Spaziali (IAPS),
Via del Fosso del Cavaliere, 100, 00133 Roma, Italy*

²*Istituto Nazionale di Fisica Nucleare (INFN), Sezione di Tor Vergata,
Via della Ricerca Scientifica 1, 00133 Roma, Italy*

³*Istituto di Scienza e Tecnologie della Informazione (ISTI), Consiglio Nazionale delle Ricerche (CNR),
Via G. Moruzzi 1, 56124 Pisa, Italy*

⁴*Dipartimento di Fisica, Sapienza Università di Roma, Piazzale Aldo Moro 5, 00185 Roma, Italy*

⁵*Agenzia Spaziale Italiana (ASI), Centro di Geodesia Spaziale (CGS),
Contrada Terlecchia, 75100 Matera, Italy*

(Received 16 July 2023; accepted 9 January 2024)

17
18
19
20
21
22
23
24
25
26
27
28
29
30
31
32
33
34

This paper introduces the main problems related to the modeling of the effects of nongravitational perturbations on satellites of the Galileo FOC constellation. The problem is addressed from the point of view of the scientific objectives of the Galileo for Science (G4S_2.0) project. These objectives are reflected in a set of fundamental physics measurements that will exploit the orbits and atomic clocks aboard the Galileo satellites, in particular the GSAT-0201 and GSAT-0202 satellites characterized by elliptical orbits, and not by almost circular orbits such as in the case of the remaining satellites of the constellation. The main focus is on the modeling of the direct solar radiation pressure, the largest nongravitational perturbation on GNSS satellites. After an in-depth presentation of the main nongravitational perturbations of interest, and of the models currently in use in the literature for their consideration, the work focuses on the amplitudes of the different effects and, with particular attention, on their intrinsic knowledge. Finally, two different models are introduced for the structure of the Galileo satellite specially developed for the objectives of G4S_2.0. The first is a simple model of the box-wing type, developed on the basis of the information currently available on the characteristics of the satellite. The second is a 3D model of the Galileo spacecraft, somewhat sophisticated due to the richness of the details on the structure and the various elements that make up the surfaces of the satellite. The activities carried out and in progress with these models and those planned with their subsequent updated versions are described.

DOI:

I. INTRODUCTION

35
36
37
38
39
40
41
42
43
44
45
46

The Galileo for Science (G4S_2.0) project [1–6], funded by the Italian Space Agency (ASI), aims to perform a set of gravitational measurements mainly using the two Galileo satellites GSAT-0201 and GSAT-0202 exploiting the relatively high eccentricity (≈ 0.16) of their orbits with respect to that (≈ 0) of the other satellites of the full operational capability (FOC) constellation. These two satellites have been already considered in 2018 by both ZARM [7] and SYRTE [8] for a new measurement of the gravitational redshift that has improved the 1976 measurement of Gravity Probe A (GPA) [9,10] by a factor between

47
48
49
50
51
52
53
54

4 and 6 respectively, see also [11,12] for more recent results. In fact, from an accurate analysis of the orbits and clocks of these two Galileo satellites, a set of relativistic tests can be performed with the objectives of comparing the predictions of Einstein’s theory of general relativity [13] with those of other gravitational theories [14] concerning, mainly, the motion of a “test” particle along a geodesic of space-time and the time dilation of the on-board clocks.

55
56
57
58
59
60
61

G4S_2.0 has four main objectives in fundamental physics plus three other main objectives that are mainly linked, but not only in truth, to technical aspects of the Galileo FOC constellation and of Global Navigation Satellite System (GNSS) satellites in general. The objectives in the field of fundamental physics are: (i) providing a new measurement of gravitational redshift; (ii) measuring

*david.lucchesi@inaf.it

the relativistic precessions of the orbits of the two satellites GSAT-0201 and GSAT-0202; (iii) placing constraints on the possible presence of dark matter in our Galaxy; (iv) providing the detection of gravitational waves. The last two objectives involve the use of the entire constellation of the Galileo FOC satellites. The other three objectives are: (v) realize a relativistic positioning system; (vi) developing new models for nongravitational forces; and (vii) realizing a new accelerometer concept for a next generation of Galileo satellites.

Three Italian research institutes are involved in G4S_2.0: Center for Space Geodesy (ASI-CGS) in Matera, Istituto di Astrofisica e Planetologia Spaziali (IAPS-INAF) in Roma and Politecnico (POLITO) in Torino.

In this work we will focus on point (vi) above and, in particular, on the direct solar radiation pressure (SRP), the largest nongravitational perturbation (NGP) on the orbit of Galileo FOC satellites and in general of all satellites of the GNSS. Indeed, the nonoptimal modeling of SRP is currently the main source of error in determining the orbits of GNSS satellites. The complex shape of these satellites (bus and wings) combined with their particular attitude law—which requires the face of the satellite that collects the different antennas to communicate with the ground stations to continuously point to the nadir while the face near the atomic clocks must look toward deep space, and finally the array of solar panels must continuously point toward the Sun for energy reasons—make the modeling of this perturbation and its optimal insertion into the precise orbit determination (POD) process a nontrivial issue. We also underline that studies like the present one, aimed at improving the modeling of the orbits of the satellites of the Galileo constellation, are of some importance for ESA in the light of future programs that foresee the use of Galileo satellites for increasingly significant purposes, as in the fields of earth sciences (such as geodesy, geophysics, and remote sensing), fundamental physics, astronomy, and time metrology [15].

The work we describe in this paper is the first of two works that we present in this issue of the journal. These works concern some of the activities currently underway at the IAPS-INAF Institute in Roma. In particular, in this paper we will focus on the NGPs models currently developed within the GNSS community and we introduce a 3D-CAD of a Galileo FOC that we have built and that we plan to use in the near future for modeling these nonconservative forces. In this regard, the 3D-CAD will be the basis for the construction of a finite element model (FEM) of the spacecraft. Indeed, the development of the FEM requires a better knowledge of the optical and thermal properties with respect to those currently available in the Galileo metadata of the European Space Agency (ESA). In the meantime we have also developed a box-wing model for these satellites based on the information contained in the Galileo metadata of ESA. In a second paper we will

present the results obtained for the direct SRP from the application of the box-wing model together with some preliminary POD for the Galileo FOC satellites.

With a view to achieving the ambitious objectives of G4S in the field of fundamental physics measurements, we underline the importance of developing a dynamic model of the main gravitational and nongravitational perturbations on the Galileo satellites which is extremely robust and reliable. This will significantly improve the determination of their orbits and related products, such as the estimation of the clock-bias of the on-board atomic clocks.

Consequently, this paper is organized in three parts. In the first we will focus on and discuss the main peculiarities and drawbacks of current models developed for the modeling of the NGPs of GNSS satellites. In the second part we provide an estimate of the accelerations due to the main NGPs as well as an estimate of their uncertainty. Finally, in the third part of the paper we introduce our preliminary models for the Galileo FOC satellites to manage the perturbing effects due to the main NGPs. To this end, the results of the analyzes on the state of the art of the NGPs models developed in the first part of this work were fundamental.

Specifically, the rest of the paper is organized as follows. In Sec. II, we first provide a classification of the main NGPs acting on GNSS satellites. In Sec. III, the state-of-the-art of the modeling of NGPs for GNSS satellites is presented together with their main criticalities. Special care is devoted to the Galileo constellation. In Sec. IV, the order-of-magnitudes of the main NGPs on Galileo FOC satellites are provided with an estimate of their corresponding uncertainties. In Sec. V, we provide our first models for the Galileo FOC satellite to be used for calculating the accelerations produced by the main NGPs. Finally, in Sec. VI our conclusions and recommendations are provided.

II. NGPs CLASSIFICATION

The improvements over time of the POD of the satellites belonging to the constellations of the GNSS, starting from the GPS one, has highlighted, since several years, the complex and subtle effects of the NGPs on their orbit and, consequently, the need to account properly for their perturbing effects to further improve the POD of these satellites at the current level of the microwave-ranging accuracy/precision [16–20]. In the case of GNSS, the management of NGPs is further complicated, as said, by the complex shape of these active satellites, compared, for example, to passive satellites, which do not have solar panels, motors and antennas. The POD improvements are truly significant for the multiplicity of products obtained from the analysis of the orbits of these satellites. These products may be classified, at a higher level, into four main categories:

- (1) Positioning.
- (2) Timing.

171 (3) Geophysics.
 172 (4) Fundamental physics.
 173 These high-level products are, of course, intimately linked
 174 to each other and not independent, having in common the
 175 precise knowledge of the orbits of the satellites, that is, of
 176 their ephemerides. Among the parameters that control the
 177 size of the NGPs relative to the gravitational perturbations
 178 is the area-to-mass ratio A/M of a spacecraft. In the case
 179 of an artificial satellite around the Earth this quantity is
 180 relatively high, between 0.01 and 0.001 m^2/kg , while it is
 181 several orders of magnitude smaller for a natural body
 182 (being inversely proportional to its radius for a homo-
 183 geneous body with uniform density). Consequently, in the
 184 case of a natural body the NGPs are usually negligible and
 185 its motion is usually studied by celestial mechanics within
 186 the Hamiltonian formalism of conservative forces. Of
 187 course, there are a few important exceptions: as the non-
 188 gravitational thrust acting on some comets and the decel-
 189 eration of the Moon along its orbit around the Earth due to
 190 energy dissipation produced by the tides raised by the
 191 Moon on the Earth's seas [21,22]. Conversely, for the
 192 artificial satellites such perturbations are not negligible if
 193 their orbits are tracked very precisely, and the approaches
 194 of "dirty" celestial mechanics are necessary to account for
 195 the effects due to these nonconservative forces [23].

196 Indeed, there are three possible approaches to account
 197 for the perturbing effects of the NGPs on a spacecraft:

- 198 (1) Model as better as possible their complex effects.
- 199 (2) Measure with a high-sensitive accelerometer their
 200 accelerations.
- 201 (3) Use a drag-free satellite.

202 Within G4S_2.0 we are interested to the first two
 203 approaches. In particular, in this paper we will concentrate
 204 only in the first point. Our goal is to define the current limits
 205 of the dynamical model for the NGPs, as well as those of
 206 the best possible dynamic model that can in principle be
 207 developed for GNSS, in particular for the Galileo con-
 208 stellation, to manage the NGPs so as to obtain the best
 209 possible POD based on the current tracking technologies
 210 of their orbits [24–28]: i.e., microwave and satellite laser
 211 ranging (SLR) [29].

212 As underlined in the previous section, this activity is
 213 carried out with a view to future measurements in the field
 214 of fundamental physics that we plan to make by exploit-
 215 ing a better knowledge of the orbits of these satellites.
 216 However, this activity will also help us to define the main
 217 characteristics of an onboard accelerometer, such as its
 218 sensitivity and measurement bandwidth, to be considered
 219 as a new payload for a next generation of Galileo
 220 satellites to further improve the performance of the
 221 Galileo constellation.

222 In the following subsections, a classification of the main
 223 NGPs will be presented with the aim of defining the
 224 complex panorama of perturbative effects at play and
 225 therefore defining the strategy to be followed to take into

account, through new models, of their effects on the orbit of
 Galileo satellites. Conversely, in Sec. III a description of the
 main models currently used to account for their perturbing
 effects will be presented.

A. Classification of the nongravitational perturbations 230

In the following we classify the NGPs on the Galileo
 satellites based on their source. In this case we need to
 consider three different sources:

- (1) Sun. 234
- (2) Earth and its environment. 235
- (3) Spacecraft itself. 236

237 However, it is important to emphasize that the perturbations
 238 that result from these sources are not completely indepen-
 239 dent. For instance, just to give two important examples, the
 240 effects of the Earth's atmosphere depend significantly on
 241 solar activity and its variations, while the terrestrial albedo
 242 depends on both solar radiation and clouds cover. As is well
 243 known from the literature, the LAGEOS geodynamic
 244 satellites [30] have played and still plays a fundamental
 245 role in the fields of geophysics and space geodesy, as well
 246 as in that of fundamental physics [31–38], and numerous
 247 refined models for the NGPs acting on their surface have
 248 been developed to improve their POD results in these areas.
 249 Consequently, a comparative analysis of the state of the
 250 art between Galileo satellites (or GNSS in general) with
 251 LAGEOS satellites will be provided below whenever
 252 deemed useful.

1. NGPs due to the Sun 253

254 The perturbation of the visible solar radiation on a
 255 spacecraft may be subdivided in the following physical
 256 effects:

- (1) Direct SRP. 257
- (2) Yarkovsky-Schach. 258
- (3) Asymmetric reflectivity. 259
- (4) Poynting-Robertson. 260

261 The direct SRP represents the largest NGP on a satellite
 262 of the GNSS and, in principle, the "easiest" to model. The
 263 perturbation arises by the interaction of the solar light with
 264 the surfaces and elements of the spacecraft and results in a
 265 momentum transfer to the satellite. The eclipses from the
 266 Earth plays a significant role in order to correctly account
 267 for the orbital effects produced by this perturbation [23,39].
 268 The SRP is responsible of long-term effects on the orbital
 269 elements.

270 The Yarkovsky-Schach effect arises by the modulation
 271 of the SRP when the satellite enters and exits from the
 272 eclipses and depends on the thermal inertia of the spacecraft
 273 surfaces and elements and by its attitude in space. This
 274 combination produces a nonuniform distribution of temper-
 275 ature across the satellite surface, with a resultant perturbing
 276 acceleration that does not average out during an orbital
 277 revolution and with long-term effects on the orbital

278 elements. This effect is well known in the case of the two
 279 LAGEOS satellites [40–50]. In the literature of GNSS, this
 280 perturbation is not explicitly considered, at least in the
 281 above description, but falls (in part) within the thermal
 282 reradiation from the spacecraft.

283 The Asymmetric reflectivity arises from a possible
 284 difference in the reflectivity of the various part of the
 285 satellite and it depends on the attitude of the satellite. This
 286 effect has been investigated in the past in the case of the two
 287 LAGEOS satellites [43,44,47,50–53].

288 The Poynting-Robertson effect [54–56] arises from the
 289 reradiation of the solar light absorbed by the spacecraft and
 290 assumed to be reradiated isotropically in its own frame of
 291 reference. The light emitted in the direction of motion is
 292 blue shifted and carries away more momentum and energy
 293 than the light emitted in the opposite direction, conse-
 294 quently a reaction force appears that decelerate, in princi-
 295 ple, the spacecraft. In the case of LAGEOS this effect was
 296 investigated by [40].

297 *2. NGPs due to the Earth and its environment*

298 The perturbations due to the Earth and its environment
 299 may be subdivided in the following physical effects:

- 300 (1) Albedo.
- 301 (2) Infrared radiation pressure.
- 302 (3) Neutral drag.
- 303 (4) Charged drag.
- 304 (5) Earth-Yarkovsky.
- 305 (6) Poynting-Robertson.

306 The main effects on the orbit of a spacecraft are due to the
 307 indirect SRP, i.e., to the Earth’s albedo perturbation, and to
 308 the infrared radiation pressure. The perturbation arises by
 309 the interaction of the visible solar light with the Earth’s
 310 surfaces and its complex anisotropic reflection.

311 In the case of a satellite in a low Earth orbit (LEO) the
 312 perturbing effects of the neutral atmosphere are significant
 313 and may compete with the perturbations due to the albedo
 314 and even with those due to the direct SRP. Again, the
 315 eclipses of the satellite play a significant role in the analysis
 316 of almost all these effects [23,57].

317 In the case of the radiation coming from the Earth,
 318 while the direct effects of the infrared radiation (long-
 319 wavelengths) may well be approximated by a few zonal
 320 harmonics (i.e., with no longitudinal dependency) [58], the
 321 day/night asymmetry makes this more difficult for the
 322 albedo, i.e., for the visible radiation which is reflected and
 323 diffused by the Earth’s surface and atmosphere. Actually,
 324 the intensity and direction of the force are complex
 325 functions of position and time, since the local optical
 326 behavior of the Earth’s surface and atmosphere is highly
 327 variable, related both to surface composition and morpho-
 328 logical and to meteorological and seasonal effects [59].

329 Therefore, long-term effects of the albedo perturbation
 330 on a satellite are complex and subtle, since they depend
 331 in a critical way on the asymmetry between the Earth’s

332 northern and southern hemispheres, resulting both from
 333 the different sea/land distribution and from seasonal
 334 phenomena (e.g., cloud and snow cover). In particular,
 335 the anisotropically reflected radiation (i.e., not symmet-
 336 rically distributed around the local zenith) from a surface
 337 element (especially in the case of oceans), produces long-
 338 term effects on the satellite orbit. In the case of the two
 339 LAGEOS a very reach literature on this subject has been
 340 produced [40,47,50,51,57,60–64].

341 In the case of GNSS, the albedo perturbation represents
 342 the most important, in magnitude, to be considered after the
 343 direct SRP [65,66]. However, Earth radiation data from
 344 dedicated satellites—in different band of the spectrum,
 345 from long-waves flux to short-waves flux—allows us to
 346 improve the modeling of both the Earth’s visible and
 347 infrared radiation. In particular, data from the CERES
 348 (Clouds and the Earth’s Radiant Energy System) [67]
 349 database are extensively used in the literature.

350 The neutral drag perturbation is due to the collisions
 351 between the satellite and the particles of the Earth’s
 352 atmosphere along its trajectory. In the case of LAGEOS-
 353 type satellites this perturbation has been well investigated
 354 in the literature [40,68–71]. As previously underlined, the
 355 neutral drag perturbation represents a very important effect
 356 for LEO satellites [72], but may be fully neglected for
 357 GNSS, because of their high altitude.

358 The interaction of a spacecraft with the surrounding
 359 atmosphere is not limited to the direct collisional effects
 360 with the particles but also to possible charged drag effects.
 361 These arises by the interaction of a charged satellite with
 362 the particles of the plasmasphere. Indeed, as consequence
 363 of the Earth’s magnetic field, the Earth’s is surrounded by
 364 a toroidal region where charged particles are trapped to
 365 move under the Lorentz force. Consequently, a charged
 366 drag arises due to the Coulombian interaction between the
 367 charged satellite and the charged particles. This kind
 368 of effect is strongly influenced by the eclipses, because
 369 of the corresponding variation of the photoelectric effect
 370 produced by solar radiation. While this effect has been
 371 investigated in the case of the LAGEOS satellites
 372 [40,50,68,70,73], it seems that this effect has never been
 373 considered in the GNSS literature.

374 Similarly to the Yarkovsky-Schach effect, the Earth-
 375 Yarkovsky effect arises from the anisotropic distribution of
 376 temperature produced on the satellite by Earth’s radiation,
 377 in particular from infrared radiation. The effect depends
 378 from the thermal inertia of the satellite surface, in particular
 379 from the corner cubes retroreflectors (CCRs), and from its
 380 attitude in space [49,73,74].

381 The Poynting-Robertson is the same as that described in
 382 previous section but produced by the Earth’s radiation [40].

383 *3. NGPs due to the spacecraft*

384 An active spacecraft, such as one of the GNSS, is itself
 385 responsible for producing NGPs of thermal origin.

386 The knowledge of the overall temperature distribution of
 387 the satellite is therefore of fundamental importance to
 388 account correctly for this kind of effects. Moreover, in
 389 addition to these thermal accelerations we must consider
 390 the thrust acceleration produced by the antennas and by
 391 maneuvers. Consequently, following the main literature in
 392 this field [75–78] we can consider the following main
 393 disturbing sources:

- 394 (1) Radiation of thermal blankets.
- 395 (2) Radiation from the radiators.
- 396 (3) Solar panels thermal radiation.
- 397 (4) Thermal radiation of excess solar array power
 398 (shunt).
- 399 (5) Antennas radiation.
- 400 (6) Maneuvers.
- 401 (7) Mass variation.
- 402 (8) Sloshing.

403 For the GPS block IIR satellites it was pointed out [77] that:
 404 “The solar array and shunt thermal radiation forces are the
 405 next lowest, representing just under 1 percent of the total
 406 each, but provide a nearly constant value about the orbit.
 407 Although the magnitudes are similar, these forces are
 408 applied in opposite directions and nearly cancel each other
 409 out,” therefore, considering these thermal perturbations
 410 explicitly negligible with respect to the direct and indirect
 411 solar radiation pressure. Following [77] in the case of GPS
 412 block IIR the following explanation was given:

- 413 (1) Radiation of thermal blankets:
 - 414 (i) Exterior body blankets absorb solar radiation
 415 and immediately reradiate it back to space,
 416 preventing excessive heating of the vehicle.
 417 The reradiation is diffuse emission of the
 418 absorbed radiation. The process of absorption
 419 and reradiation is equivalent to diffuse reflection.
 420 The surface body properties are adjusted to
 421 model reradiation as diffuse reflectivity and the
 422 results are included with the visible solar forces
 423 instead of the thermal forces.
- 424 (2) Radiation from the satellite radiators:
 - 425 (i) Space vehicle internal components generate
 426 heat that must be dumped to space to prevent
 427 excessive temperatures.
- 428 (3) Solar panels thermal radiation
 - 429 (i) The solar arrays and shunt dissipaters require
 430 special modeling due to the conversion of
 431 electrical power. The reradiation force accounts
 432 for the solar array radiating heat from both the
 433 front and back sides.
- 434 (4) Thermal radiation of excess solar array power (shunt)
 - 435 (i) The shunt energy dissipation is the difference
 436 between the energy provided by the array and
 437 the energy required by the on-board subsystem
 438 components. The shunt force is calculated from
 439 this dissipated power. The shunts dissipate
 440 energy from the anti-Sun side only.

- 441 (5) Antennas radiation
 - 442 (i) RF radiation force is included with the radiator
 443 forces as a steady state force throughout
 444 an orbit.
- 445 (6) Maneuvers
 - 446 (i) Reference [77] mentioned the maneuvers, but
 447 with no direct consideration of their effects.

448 Currently, to our knowledge, in the case of Galileo satellites,
 449 there are no dedicated in-depth studies for the above effects.
 450 Only, point 1. is usually taken into consideration in the
 451 way suggested by [77]. However, even in the case of GPS
 452 satellites, the studies mentioned above cannot be considered
 453 exhaustive, as they are characterized by simplifications and
 454 approximations, sometimes unavoidable, and the models
 455 developed are mainly based on empirical terms.

456 As specified above, active satellites, such as GNSS
 457 satellite, have antennas emitting a significant radiated
 458 power. In this case the spacecraft is also affected by a
 459 thrust due to antenna, the so-called antenna thrust, a small
 460 acceleration pointing into the direction opposite to the
 461 antenna. Indeed, the transmission of GNSS navigation
 462 signals is carried out by sending microwave power toward
 463 the Earth by the antenna. Being typically fixed for GNSS
 464 (Galileo as well [79]), the boresight of the antenna must
 465 always be directed toward the Earth’s center to provide a
 466 correct signal strength (i.e., the navigation message) and an
 467 optimized coverage. In order to evaluate such an effect, the
 468 knowledge of the transmitted power and the spacecraft
 469 mass are requested, in addition to the orbit height. Indeed,
 470 the modeling of such a term can be carried out as follows,
 471 according to [23]:

$$\mathbf{a}_{\text{thrust}} = \frac{P}{Mc} \frac{\mathbf{x}}{|\mathbf{x}|} \quad (1)$$

472 where P is the transmitted power, M is the spacecraft mass,
 473 c the speed of light in vacuum, and \mathbf{x} is the position vector
 474 of the satellite. In this modeling it is assumed that the
 475 antenna boresight is directed toward the Earth’s center and
 476 the antenna has a radiation pattern with a narrow-beam and
 477 a rotationally symmetric gain [80].
 478

479 All the aspects mentioned above will need to be
 480 deepened and well defined when it becomes necessary
 481 to develop a reliable thermal model of the satellite. For this
 482 to be indispensable, optimal modeling not only of the
 483 direct solar radiation pressure, but also of the albedo and
 484 terrestrial infrared radiation must be achieved.

485 III. NGPs MODELS FOR GNSS SATELLITES

486 Considering the NGPs modeling, two main approaches
 487 may be considered:

- 488 (1) Build a refined model for the spacecraft in such a
 489 way to compute the effect of the interaction of
 490 each surface element, as well as of the appendices,

491 with the external (or even internal) radiation sources.
 492 The corresponding perturbing accelerations will be
 493 used in the POD for the data reduction.

494 (2) Apply the tools of celestial mechanics to find which
 495 component of the perturbing force is really signifi-
 496 cant, on the basis of the tracking technique and time
 497 of accumulation of its effects on the orbit. Develop
 498 an analytic model (usually a simplified model) to be
 499 included in the dynamical model used in the POD
 500 for the data reduction.

501 In this section these two approaches will be considered and
 502 described in their guiding elements on the basis of the state
 503 of the art of the literature and of the POD procedures typical
 504 of GNSS. Our main objective in this context is to build, on
 505 the basis of the information collected, a new finite element
 506 model (FEM) of the Galileo FOC satellites (see Sec. V) that
 507 can meet the ambitious objectives of G4S_2.0: that is to
 508 improve the POD of the satellites in order to use their orbits
 509 for fundamental physics measurements.

510 A. General aspects

511 Usually, in the literature of the NGPs modeling, the
 512 second approach has been followed, by fixing some of
 513 the parameters of the model (these are “considered param-
 514 eters”) and estimating the other in the POD, as for the
 515 radiation coefficient C_R or the drag coefficient C_D (these
 516 are adjusted parameters). Sometimes, these analytical
 517 models are accompanied by the use of empirical
 518 accelerations to better absorb some effects not currently
 519 modeled [16,81–84], as in the case of the empirical CODE
 520 orbit model (ECOM) and its subsequent versions. In a few
 521 cases also stochastic accelerations or velocities are intro-
 522 duced to absorb the orbit mismodeling.

523 Certainly, the use of empirical accelerations does not
 524 allow to obtain a physical description of the many
 525 perturbative effects involved. Therefore, such empirical
 526 accelerations must be introduced with extreme care when
 527 it is deemed necessary, and with the main objective of
 528 reducing the orbital residuals in the POD of the satellites.
 529 Anyway, their use should be avoided whenever the
 530 correct physical interpretation of a given effect is
 531 requested, as for instance in the case of the origin of
 532 the so-called Y-bias acceleration or when fundamental
 533 physics measurements are considered.

534 Presently, the best representation of the second approach
 535 can be considered a simple (or simplified) box-wing
 536 (S-BW) model. With a S-BW model we mean the consid-
 537 eration of a number of flat surfaces of the spacecraft
 538 through which we are able to estimate the SRP accel-
 539 erations acting on it, once the average optical coefficients of
 540 each surface have been set. Of course, at the same time, the
 541 development of a BW model represents a first step toward
 542 the realization of the first approach previously cited, i.e.,
 543 the development of a FEM for the satellite. The develop-
 544 ment of a really refined FEM requires:

- 545 (1) A very accurate representation of the complex 545
 546 geometry of the spacecraft. 546
- 547 (2) The knowledge of the physical characteristics—such 547
 548 as optical (in the visible and in the infrared) and 548
 549 thermal—of each kind of surface and element 549
 550 (antenna, appendices, CCR, insulators, radiators, 550
 551 etc.) that constitute the spacecraft, also including 551
 552 the internal ones. 552
- 553 (3) The knowledge of how these characteristic (espe- 553
 554 cially the optical ones) evolve in time and how 554
 555 they are function, for instance, of the illumination 555
 556 conditions. 556
- 557 (4) To account for multiple reflections. 557
- 558 (5) The knowledge with high accuracy of the spacecraft 558
 559 attitude with respect to the Earth and to the Sun 559
 560 during its orbital revolution around the Earth, as well 560
 561 as during the (unavoidable) orbital maneuvers. 561
- 562 (6) For a given attitude, we need to be able to model the 562
 563 mutual shadowing effects produced by the space- 563
 564 craft surfaces and appendices, in order to account for 564
 565 umbra and penumbra effects. 565

566 Consequently, the development and fruitful use of a refined 566
 567 and complete FEM of a spacecraft, based on the application 567
 568 of the ray-tracing technique, is a truly daunting task. In fact, 568
 569 until the last years, this first approach in modeling has not 569
 570 been pursued, due to the numerous complexities mentioned 570
 571 above, and also due to the numerical integration and the 571
 572 time required to perform all the detailed interactions, which 572
 573 must include multiple reflections, with umbra and penum- 573
 574 bra calculations, the knowledge of the optical properties 574
 575 of the surfaces and the correct satellite attitude in space. 575
 576 Consequently, the $\approx 1\%$ precision reachable (in principle) in 576
 577 the modeling of the direct solar radiation pressure by means 577
 578 of a reliable FEM was indeed considered illusory [23], also 578
 579 in relation to the lower quality of tracking in the past. 579

580 However, in the last two decades, thanks to the improve- 580
 581 ments in computing power, together with the development 581
 582 of algorithms and dedicated software for ray-tracing 582
 583 techniques, or by test particle Monte Carlo (TPMC) 583
 584 approach [85–88], even with a normal *personal computer* 584
 585 it is now possible to produce a satellite FEM able to 585
 586 improve the modeling of NGPs, starting from the SRP, the 586
 587 largest NGP on GNSS spacecraft. 587

588 Indeed, first, as previously introduced, several BW models 588
 589 have been developed—with different (but still limited) level 589
 590 of sophistication—for GNSS spacecraft [17,66,89–92] and, 590
 591 in particular for the Galileo ones [20,93–95]. 591

592 Regarding the construction of a FEM, this possibility has 592
 593 been considered in numerous papers in the GNSS literature 593
 594 to improve the modeling of the SRP and secondly of the 594
 595 thermal effects [17,75,76,89,90,93,94,96–99]. However, 595
 596 although the main ingredients for developing a reliable 596
 597 FEM have been well highlighted in the cited literature, 597
 598 especially in the most recent works, it seems that a refined 598
 599 FEM has never been developed and tested and routinely 599

600 applied in the POD of GNSS satellites, or at least the
 601 corresponding results and applications have never been
 602 published. We think this is closely related to how the
 603 so-called *precise orbits* are currently determined by the
 604 International GNSS Service (IGS). These are in fact,
 605 together with the *clock-bias*, one of the main products that
 606 today are obtained from the analysis of the orbits of GPS
 607 and GLONASS satellites. Since these are determined over a
 608 short time interval, the NGPs perturbations do not have
 609 time to accumulate sufficiently and what is not modeled is
 610 absorbed by estimating empirical terms. We will return to
 611 these aspects later, see Secs. III B 2 and III B 5.

612 Concerning the use of a FEM for Fundamental
 613 Physics applications and, in particular, in the case of
 614 the measurement of the gravitational redshift, both
 615 ZARM and SYRTE have done some activity in this
 616 direction. Indeed, a FEM of a Galileo FOC has been
 617 developed by ZARM and the results for the SRP have
 618 been used by ESA in their POD for the measurement of
 619 the gravitational redshift performed in 2018 [7], but no
 620 results have been published in this regard at the time of
 621 this measurement (Benny Rievers personal communica-
 622 tion) and no mention of the FEM is reported in [7]. The
 623 FEM model developed by ZARM was published only
 624 in 2023 [100]. This model has good performance, well
 625 superior to those of a S-BW, but cannot be considered a
 626 refined FEM of the Galileo FOC satellite since not based
 627 on sufficiently detailed information regarding the optical
 628 properties of the various components of the satellite and
 629 also not having any information on the temperature
 630 distribution on the satellite (Benny Rievers personal
 631 communication). Consequently, the accuracy that can
 632 be achieved with a FEM for modeling the SRP for a
 633 Galileo FOC satellite has not yet been defined. However,
 634 the quality of the FEM described in [100] is remarkable
 635 under several aspects.

636 In the case of the measurement of the gravitational
 637 redshift performed by SYRTE [8], in their supplementary
 638 material [101] it is explicitly written: *For direct and*
 639 *indirect solar radiation pressure (SRP) modeling of the*
 640 *Galileo FOC (full operational capability) satellites, a*
 641 *numerical raytracing model based upon the geometrical*
 642 *form of the surface of the spacecraft and the optical*
 643 *characteristics of each component is employed.* The
 644 authors refers, quoting the Ref. [102], to the software
 645 Aerodynamics and Radiation Pressure Analysis (ARPA)
 646 developed at the University of Padua in Italy for
 647 the analysis of the nongravitational forces acting on
 648 GOCE [103]. Again, there is no clear explanation for
 649 the quantitative improvement in the POD of a Galileo FOC
 650 satellite using such software over the usual models.

651 B. Current main models for the NGPs

652 Based on the extensive literature of satellites belonging
 653 to the GNSS, and also regarding the analysis of their orbits

for applications in the fields of geophysics and space
 geodesy, as for:

- (i) Earth rotation parameters. 656
- (ii) Global scale. 657
- (iii) Geocenter coordinates. 658

See for instance [104,105], we can summarize the current
 models for the NGPs in the following typologies (also
 following a chronological order in their development):

- (1) Cannonball. 662
- (2) Empirical accelerations. 663
- (3) Pseudo stochastic pulses. 664
- (4) S-BW. 665
- (5) BW with empirical accelerations. 666
- (6) BW with adjusted coefficients. 667
- (7) FEM. 668

669 1. Cannonball model

The cannonball model represents a very rough solution
 to take into account the shape of a satellite. In the case of
 the SRP, it models the average cross section seen by the Sun
 and with average optical coefficients parametrized by a
 radiation coefficient (of course, the cross section seen by
 the Earth is different from this average value, because of the
 solar panels orientation toward the Sun, and it is subject to a
 periodic variation). The cannonball model accounts for the
 average (bulk) acceleration on the spacecraft but with a low
 spectral content, practically only for an effect at the orbital
 period of the spacecraft. Therefore, many features are
 lost when using a simple cannonball model. In the case
 of GPS literature, it was usually used as an *a priori* model
 complemented by estimates of empirical terms along the
 axes of the spacecraft (+Z toward the Earth, +X toward
 the half plane that contains the Sun, and +Y completes the
 right-handed system and point along the solar panels axis).

We refer to the accompanying paper for the application
 of the cannonball model to the POD of the Galileo FOC
 satellites.

690 2. Empirical models

In the literature of GNSS, starting from GPS and
 GLONASS, the empirical models have been, and still are,
 very successful to account for the SRP perturbation [16,82].
 The empirical model is based on the results acquired at the
 center of orbit determination in Europe (CODE) since 1992
 in the context of several activities regarding the IGS. Within
 CODE the direct SRP acceleration is modeled as:

$$\mathbf{a}_{\odot} = \mathbf{a}_{\odot,0} + D(u)\hat{\mathbf{s}} + Y(u)\hat{\mathbf{e}}_{\mathbf{Y}} + X(u)\hat{\mathbf{e}}_{\mathbf{X}}. \quad (2)$$

The first term, $\mathbf{a}_{\odot,0}$, represents the acceleration as given by
 an *a priori* model for the SRP (usually the ROCK model
 used by GPS, see, e.g., [76,106]), $\hat{\mathbf{s}}$ is the unit vector from
 the spacecraft center of mass to the Sun (indicated as $\hat{\mathbf{e}}_{\mathbf{D}}$
 in [16]), $\hat{\mathbf{e}}_{\mathbf{Y}}$ is the unit vector along the spacecraft solar panel
 axis, $\hat{\mathbf{e}}_{\mathbf{X}} = \hat{\mathbf{e}}_{\mathbf{D}} \times \hat{\mathbf{e}}_{\mathbf{Y}}$ defines a right-handed reference system,

705 and u represents the argument of latitude of the spacecraft
 706 ($u = \omega + f$, with ω the argument of pericenter and f the true
 707 anomaly). Each of the accelerations terms $D(u)$, $Y(u)$ and
 708 $X(u)$ represents an empirical acceleration constituted by a
 709 constant and two periodic once-per-revolution accelerations
 710 (sine and cosine terms):

$$\begin{cases} D(u) = D_0 + D_s \sin u + D_c \cos u \\ Y(u) = Y_0 + Y_s \sin u + Y_c \cos u \\ X(u) = X_0 + X_s \sin u + X_c \cos u \end{cases} \quad (3)$$

723

$$\begin{cases} D(u) = D_0 + \sum_{i=1}^{n_D} \{D_{2i,c} \cos 2i\Delta u + D_{2i,s} \sin 2i\Delta u\} \\ Y(u) = Y_0 \\ B(u) = B_0 + \sum_{i=1}^{n_B} \{B_{2i-1,c} \cos(2i-1)\Delta u + B_{2i-1,s} \sin(2i-1)\Delta u\} \end{cases} \quad (4)$$

724 where we have introduced the symbol B instead of X ,
 725 following the notations of [18], and where the argument
 726 of latitude $\Delta u = u - u_\odot$ of the satellite with respect to that
 727 of the Sun has replaced the argument of latitude u of the
 728 satellite. It is important to stress that the B -axis does not
 729 coincide (in general) with an axis of the spacecraft, and so it
 730 does not correspond to the orientation of the spacecraft bus;
 731 it varies in a space limited by the $\pm Z$ and $+X$ axes.

3. Pseudostochastic pulses

732

733 The so called pseudo-stochastic pulses were firstly
 734 introduced by [16] and allow to estimate instantaneous
 735 velocities changes of a satellite in predefined directions
 736 (usually radial, cross-track and transverse directions) at
 737 predefined epochs. This method was later generalized to
 738 allows for piecewise constant or even piecewise linear
 739 accelerations [107,108] in the POD. In the data reduction,
 740 the pseudostochastic pulses are treated as any other
 741 adjusted parameter; consequently, since the partial deriv-
 742 atives of the orbit are needed with respect to these addi-
 743 tional parameters, the normal equations may grow
 744 considerably in their size, leading to a not efficient least-
 745 squares procedure [25].

4. Box-wing model

746

747 Several box-wing models, as already highlighted, have
 748 been developed for GNSS satellites. In the case of the
 749 Galileo FOC we refer to [20,95] that have built a S-BW on
 750 the basis of the Galileo metadata [109] and following [17].
 751 The BW is obtained by considering the satellite, as a box
 752 made of flat surfaces (such as a parallelepiped or a cuboid)
 753 plus the flat wings of the solar panels. Assuming that each
 754 surface dA behaves like a linear combination of a black
 755 body, a perfect mirror and a perfect diffuser—with the
 756 corresponding optical coefficients: α (for absorption), ρ (for

712 Therefore, this model contains up to nine parameters
 713 that can be estimated over a fixed time span in order to
 714 absorb the unmodeled part of the SRP perturbation, see
 715 also [104]. More recently, the ECOM model was extended to
 716 ECOM2 [18]. The ECOM2 model considers a constant
 717 acceleration along each of the above axis, plus even periodic
 718 terms in the Sun direction (currently, twice-per-revolution
 719 terms) and odd periodic terms along the X axis (currently,
 720 once-per-revolution terms). Consequently, Eq. (3) trans-
 721 forms as:

757 specular reflection) and δ (for diffuse reflection), and such
 758 that $\alpha + \rho + \delta = 1$ —for the acceleration produced by the
 759 direct SRP we obtain the following expression [23]:

$$\mathbf{da} = -\frac{\Phi_\odot}{Mc} \left[(1-\rho)\hat{\mathbf{e}}_D + 2\left(\frac{\delta}{3} + \rho \cos \vartheta\right)\hat{\mathbf{n}} \right] dA |\cos \vartheta| \quad (5)$$

760 where Φ_\odot represents the solar irradiance, M the mass of the
 761 satellite, c the speed of light, $\hat{\mathbf{n}}$ the unit vector normal to
 762 the surface dA and ϑ the Sun zenith angle with respect to
 763 the surface normal: $\cos \vartheta = \hat{\mathbf{e}}_D \cdot \hat{\mathbf{n}}$.

764 The condition $\alpha + \rho + \delta = 1$ represents a strong
 765 assumption, which means that the absorbed light is not
 766 reemitted, that the light reflection is perfectly specular and,
 767 finally, for a given direction the intensity of the diffused
 768 light is proportional to the cosine of the angle with the
 769 normal $\hat{\mathbf{n}}$, i.e., Lambert's law holds up with a diffusion lobe
 770 of spherical shape. In the case of the model described
 771 in [20,95], as well as in [17], Eq. (5) in the case of the bus
 772 was replaced by:
 773

$$\mathbf{da} = -\frac{\Phi_\odot}{Mc} \left[(\alpha + \delta) \left(\hat{\mathbf{e}}_D + \frac{2}{3} \hat{\mathbf{n}} \right) + 2 \left(\frac{\delta}{3} + \rho \cos \vartheta \right) \hat{\mathbf{n}} \right] dA |\cos \vartheta|, \quad (6)$$

774 following the suggestion of the authors of [77], i.e.,
 775 assuming immediate thermal reradiation. In this case, we
 776 need to consider an additional contribution to the accel-
 777 eration given by the radiation that is radiated back to space
 778 according to Lambert's law:
 779

$$\mathbf{da}_{rr} = -\frac{2}{3} \alpha \frac{\Phi_\odot}{Mc} dA |\cos \vartheta| \hat{\mathbf{n}}, \quad (7)$$

780 which added to Eq. (5) gives Eq. (6). However, by doing so,
782 the validity of the previous condition:

$$\alpha + \rho + \delta = 1 \quad (8)$$

783 is still imposed, but in reality it is no longer valid in the case
785 of reemission of the absorbed radiation.

786 As for the NGPs, the authors of [20,95] have applied
787 their BW model to the direct SRP, the Earth's albedo and
788 infrared radiation and the thrust produced by the navigation
789 antenna. The POD results for this S-BW model were
790 compared with hybrid box-wing solutions, where a set
791 of empirical parameters, following the ECOM and ECOM2
792 style, were estimated in order to reduce the orbit residuals.
793 In this way, the authors were able to obtain the best solution
794 for their POD, as well as for orbit predictions and for
795 estimating geodetic parameters.

796 Finally, by means of a BW model it is possible to adjust,
797 in the POD procedure, some of the optical coefficients of
798 the surfaces with the goal to reduce the orbital residuals
799 of the satellites. This can be useful if the information on the
800 optical properties is not reliable or considered not updated.
801 Indeed, this approach was followed in part by [17] for the
802 GPS satellites (Block II/IIA and IIR) during a dedicated
803 analysis in 2007. The tracking data of the GPS were
804 obtained from CODE and two different solutions com-
805 puted: (i) one using the adjustable BW model and (ii) one
806 using the empirical model of CODE. The analyses per-
807 formed for the year 2007 focused on the difference between
808 the estimated parameters and orbits in the two cases.

809 5. Finite element model

810 The main features of a refined FEM have already been
811 introduced in the previous Sec. III A together with the
812 numerous difficulties in its reliable implementation. In the
813 following, we are interested in highlighting some of
814 the advantages that can be obtained in the future for
815 GNSS satellites through the use of a reliable FEM:

- 816 (1) A new high-precision numerical model to account
817 for the perturbative effects of direct SRP allows to
818 avoid the strong use that is currently being made of
819 empirical parameters during the POD.
- 820 (2) It would allow better modeling of perturbative
821 effects that are two orders of magnitude lower in
822 acceleration than SRP, starting from Earth's albedo
823 and infrared radiation pressure.
- 824 (3) It would pave the way for a better and more detailed
825 consideration of the numerous thermal reradiation
826 effects previously introduced, see Sec. II A.
- 827 (4) It would hopefully allow, under favorable condi-
828 tions, to take into account the perturbative effects
829 linked to the variation of solar irradiation.
- 830 (5) it would allow to provide (both directly and indi-
831 rectly) better predictions for the orbits generated by
832 IGS and by the main analysis centers.

(6) it would allow to provide a more precise and
834 accurate POD for the fundamental physics applica-
835 tions of GNSS satellites.

836 Regarding the first point, the physical reasons that
837 suggest, possibly, to avoid an intensive use of empirical
838 terms in the POD have already been highlighted in
839 Sec. III B. In fact, in addition to drastically reducing
840 its use, the FEM could limit the use of empirical terms to
841 perturbative effects in acceleration much smaller than
842 those produced by direct SRP.

843 In particular, a successful application of FEM to model-
844 ing the effects of radiation pressure from the Earth-
845 atmosphere system, second point above, would limit the
846 use of empirical terms to thermal effects.

847 As for the third point, in case we have a good knowledge
848 of the temperature distribution on the surface of the
849 spacecraft and its elements (also considering its interior,
850 with heat transport and radiation mechanisms of the
851 spacecraft structure)—distribution that strongly depends
852 (but not only, see Sec. II A) from the illumination of the
853 Sun—it would be possible in principle to calculate the
854 elementary acceleration from each surface element. This
855 would allow us to calculate the total acceleration produced
856 by the radiation emitted by the spacecraft's surface due to
857 its anisotropic temperature distribution. We refer to [98] as
858 a very good example in this direction.

859 Concerning the solar irradiance (point four), it is
860 estimated to vary in the range 0.1% ÷ 0.2% during one
861 solar cycle of about 11 years. Its contribution to the model
862 uncertainty are currently negligible with respect to the error
863 that arises from the knowledge of the optical coefficients
864 of the Galileo FOC satellites, and in general of the GNSS
865 ones. Therefore, its *a posteriori* modeling will be possible
866 and fruitful only if, before the launch of a satellite, precise
867 measurements of the optical coefficients of the various
868 surfaces and elements, and in particular of the solar panels,
869 will be made. In this regard, the law of degradation of the
870 optical coefficients and the knowledge of the satellite's
871 attitude will also play a significant role.

872 Today, the measurement uncertainties of the solar
873 irradiance are comparable with its variations over the solar
874 cycle. The irradiance variations are measured through
875 radiometers onboard dedicated satellites since 1978.
876 These measurements show a well-defined correlation
877 between the 11-year solar cycle and the solar magnetic
878 activity cycle [110].

879 The timescales on which the solar irradiance varies are
880 different depending on the physical cause that is at the
881 origin of the variation in the irradiance itself. If we restrict
882 to irradiance variations at timescales up to the solar cycle,
883 of the order of a lifetime of a typical GNSS constellation,
884 we can highlight the following timescales:

- 885 (i) From minutes to hours: the variability is driven by
886 p-modes (i.e., pressure modes due to standing sound
887 waves) and granulation (i.e., due to convection

- 888 cells in the convective zone below the Sun's photo-
 889 sphere).
- 890 (ii) From hours to days: the variability is mainly driven
 891 by sunspots (i.e., by the evolution and rotational
 892 modulation of magnetic features) and granulation or
 893 supergranulation.
- 894 (iii) From days up to ≈ 1 month (about the Sun rotation
 895 period) [111]: the variability is mainly driven by
 896 sunspots and faculae (i.e., by bright spots in the
 897 photosphere).

898 We refer to [112,113] for further details on the solar
 899 irradiance and its variations.

900 Currently, considering the magnitude of the variation in
 901 solar irradiation and also considering that the limit of a
 902 precision of 1% of a SRP model based on an FEM is in any
 903 case a very difficult task to achieve and also to maintain
 904 over time, probably the corresponding variations of the
 905 acceleration due to direct SRP, on the order of a few
 906 10^{-10} m/s², will be very difficult to model correctly. This is
 907 a case where the measurements of an accelerometer with
 908 the right sensitivity could perform better than present, and
 909 possibly future, models.

910 As for the fifth point, a reliable model for the SRP is
 911 crucial for providing more reliable predictions for the orbits
 912 of the satellites. In fact, the goodness and reliability of this
 913 model is one of the main aspects that influence the final
 914 accuracy of the predicted orbits by the IGS. Indeed,
 915 predictions, i.e., orbit propagation, represents an important
 916 issue in the current activities of the IGS.

917 A very good example is provided by ultrarapid orbits,
 918 that are very important for real-time or *quasi* real-time
 919 applications. In this case the orbits are determined by a fit
 920 of the observations (i.e., of the phase of the carrier) on a
 921 period of three days. The state vector of the satellite is
 922 estimated at the beginning of the first day.

923 The ultrarapid orbit is provided on two days files as
 924 follows: the first day consists of the observed orbit during
 925 the third daily arc, obtained by propagating the estimated
 926 state vector at the beginning of the arc of the first day; the
 927 second day of the ultrarapid orbit consists of a predicted
 928 orbit (or propagated orbit) after the third day of the POD,
 929 it corresponds to the fourth day. Than the POD process is
 930 repeated with a 6-hour shift. These are combined orbits,
 931 for the first day orbit the accuracy is about 3 cm, while for
 932 the fully predicted orbit the accuracy is about 5 cm.
 933 Clearly, in all these orbit propagation contexts, reliable
 934 models and their covariance play a crucial and irreplace-
 935 able role.

936 On the contrary, the measurements of an accelerometer,
 937 as well as the use of empirical terms, cannot provide a
 938 direct contribution to the prediction of the orbit. However,
 939 an indirect effect is possible. Indeed, the measurements of
 940 the on-board accelerometer can be used to calibrate some
 941 parameters of the NGPs models, as well as some empiri-
 942 cal terms.

The last point is the one we are most directly interested
 in. Of course, once a reliable FEM has been implemented,
 and with the most efficient approach of Ray-Tracing
 technique for our goals—being primarily interested in
 the analysis of the orbits over relatively long periods, in
 order to enhance (the unmodeled) relativistic effects of the
 secular type—the *a posteriori* analysis of the orbits is
 simpler than that necessary to obtain the orbits according to
 the procedure adopted by IGS. In this context it will be
 important to correctly define the length of the orbital arc of
 the POD of the considered satellites. This will be a function
 not only of the relativistic effect that is the subject of
 our analysis from time to time, but also of the number of
 observations available as regards the satellite laser ranging
 (SLR) technique. Indeed, full rate SLR data can be
 exploited to improve the orbit modeling during penumbra
 transitions.

However, we also believe that a study dedicated to
 understanding how to insert the values of perturbative
 accelerations of nongravitational origin, obtainable from a
 reliable FEM, into the POD procedures typical of GNSS
 analysis centers, is necessary and important.

In conclusion, by means of a reliable box-wing (R-BW)
 model and, hopefully in the future, by means of a FEM, it is
 possible to explain in principle a significant fraction of the
 disturbing effects that have been discussed above for the
 GNSS satellites and, in particular, for the Galileo ones.

Of course, the main objective still deals with the one to
 improve the model for the SRP and, subsequently, that for
 the albedo perturbation.

IV. ORDERS OF MAGNITUDE FOR THE NGPs

As already highlighted, a GNSS satellite is subject to a
 very wide range of physical perturbations of nongravita-
 tional origin in addition to those of gravitational origin. The
 latter are mainly due to the deviations of the Earth's mass
 distribution from the spherical symmetry and to third body
 effects. Even the values assumed by the various perturba-
 tive accelerations are very spread, varying on several orders
 of magnitude. In this context, the way to decide which
 perturbations are negligible is not so simple in general. An
 acceleration is not negligible in itself, but, firstly, with
 respect to the other accelerations and, second, with respect
 to the precision that can be achieved in the data reduction,
 i.e., in the satellite's POD. The POD is a function of the
 precision of the tracking observations of the position of
 the satellite, of the overall dynamical model included in the
 software used for the orbit determination and of the arc
 length used for the data reduction [114]. Of course, the
 main motivation for providing better (and even new)
 models for the various perturbations is connected with
 the significant increase in the precision of the tracking
 measurements of the satellite that have been nowadays
 reached, both for microwaves and (especially) for the laser

TABLE I. Comparison of the main gravitational accelerations (S.I. units) on LAGEOS II with the corresponding accelerations on a Galileo FOC satellite.

Physical effect	Formula	Parameter	LAGEOS II	Galileo FOC
Earth's monopole	$\frac{GM_{\oplus}}{r^2}$	$GM_{\oplus} = 3.986004418 \times 10^{14}$	2.6948	0.4549
Earth's oblateness	$3 \frac{GM_{\oplus}}{r^2} \left(\frac{R_{\oplus}}{r}\right)^2 \bar{C}_{2,0}$	$\bar{C}_{2,0} = -4.841694573200 \times 10^{-4}$	1.08×10^{-3}	3.1×10^{-5}
Low-order geopotential	$3 \frac{GM_{\oplus}}{r^2} \left(\frac{R_{\oplus}}{r}\right)^2 \bar{C}_{2,2}$	$\bar{C}_{2,2} = +2.439374598584 \times 10^{-6}$	5.4×10^{-6}	1.5×10^{-7}
Low-order geopotential	$7 \frac{GM_{\oplus}}{r^2} \left(\frac{R_{\oplus}}{r}\right)^6 \bar{C}_{6,6}$	$\bar{C}_{6,6} = +9.476848430257 \times 10^{-9}$	3.7×10^{-9}	3.0×10^{-12}
High-order geopotential	$13 \frac{GM_{\oplus}}{r^2} \left(\frac{R_{\oplus}}{r}\right)^{12} \bar{C}_{12,12}$	$\bar{C}_{12,12} = 2.422093764787 \times 10^{-9}$	3.7×10^{-11}	1.4×10^{-16}
Moon	$2 \frac{GM_{\bullet}}{r_{\bullet}^2} r$	$GM_{\bullet} = GM_{\oplus}/81.3$	2.2×10^{-6}	5.3×10^{-6}
Sun	$2 \frac{GM_{\odot}}{r_{\odot}^3} r$	$GM_{\odot} = 1.32712442099 \times 10^{20}$	9.6×10^{-7}	2.3×10^{-6}
Venus	$2 \frac{GM_{\heartsuit}}{r_{\heartsuit}^3} r$	$GM_{\heartsuit} = 0.82GM_{\oplus}$	1.2×10^{-10}	3.0×10^{-10}
Indirect oblation	$3 \frac{GM_{\oplus}}{r^2} \left(\frac{R_{\oplus}}{r}\right)^2 \frac{M_{\oplus}}{M_{\oplus}} \bar{C}_{2,0}$	$GM_{\oplus}, \bar{C}_{2,0}$	1.4×10^{-11}	1.4×10^{-11}
Dynamic solid tide	$3k_2 \frac{GM_{\bullet}}{r_{\bullet}} \left(\frac{R_{\oplus}}{r}\right)^2 \frac{R_{\oplus}^3}{r^4}$	$k_2 \simeq 0.3$	3.9×10^{-8}	1.1×10^{-9}
Dynamic ocean tide	≈ 0.1 of dynamic solid tide		3.9×10^{-9}	1.1×10^{-10}
Kinematic solid tide	$h \left(\frac{2\pi}{T_{\text{syn}}/2}\right)^2$	$h \simeq 0.30$	5.8×10^{-7}	5.8×10^{-7}
Kinematic ocean loading	$h_L \left(\frac{2\pi}{T_{\text{syn}}/2}\right)^2$	$h_L \simeq 0.05$	9.7×10^{-8}	9.7×10^{-8}
Main GR correction	$\frac{GM_{\oplus}}{r^2} \frac{GM_{\oplus}}{c^2} \frac{1}{r}$	$\frac{GM_{\oplus}}{c^2} = 4.43502804 \times 10^{-3}$	9.8×10^{-10}	6.8×10^{-11}

996 ranging ones. A possible alternative is to measure the
 997 nongravitational accelerations with an onboard accelerom-
 998 eter. However, from a general point of view, it is important
 999 to underline that the accelerometer measurements must be
 1000 considered as a complement to the models in a synergistic
 1001 approach and, consequently, should not replace the models.
 1002 In Tables I and II are shown the order-of-magnitude
 1003 of the perturbing accelerations for the current Galileo

FOC satellites (column 5) due to the main gravitational
 perturbations and the main NGPs that we have described
 above. Indeed, for completeness, the NGPs accelerations
 are compared with the Earth's monopole acceleration and
 with the main gravitational accelerations. We also consid-
 ered third-body effects and tides. The comparison is also
 extended to LAGEOS II (column 4), one of the best tracked
 satellites by the International Laser Ranging Service

TABLE II. Comparison of the main nongravitational accelerations (S.I. units) on LAGEOS II with the corresponding accelerations on a Galileo FOC satellite. The symbol (\dots) means that the acceleration is negligible, while the symbol (\neg) means that the acceleration is currently unknown (not available), since it has not yet been evaluated.

Physical effect	Formula	Parameter	LAGEOS II	Galileo FOC
Direct SRP	$C_R \frac{A}{M} \frac{\Phi_{\odot}}{c}$	$\Phi_{\odot} = 1360.8$	3.2×10^{-9}	1.0×10^{-7}
Earth's albedo	$2 \frac{A}{M} \frac{\Phi_{\odot}}{c} A_{\oplus} \frac{\pi R_{\oplus}^2}{4\pi r^2}$	$A_{\oplus} \approx 0.3$	1.3×10^{-10}	7.0×10^{-10}
Earth's infrared radiation	$\frac{A}{M} \frac{\Phi_{\text{IR}}}{c} \frac{R_{\oplus}^2}{r^2}$	$\Phi_{\text{IR}} \approx 240$	1.5×10^{-10}	1.1×10^{-9}
Neutral drag	$\frac{1}{2} C_D \frac{A}{M} \rho V^2$	$C_D \simeq 4.0, \rho \simeq 5.7 \times 10^{-18}$	2.6×10^{-13}	\dots
Charged drag	[50], Chap. 5	Species densities, floating potential	2.0×10^{-12}	\neg
Power from antennas	$\frac{P}{Mc}$	$P = 265$		1.2×10^{-9}
Solar Yarkovsky-Schach	$\frac{16}{9} \frac{A}{M} \frac{\epsilon \epsilon}{c} T_0^3 \Delta T$	$\epsilon, T_0, \Delta T$	1.0×10^{-10}	\neg
Earth Yarkovsky	$0.41 \frac{4}{9} \frac{A}{M} \frac{\epsilon \Phi_{\text{IR}} f_0}{ac} \frac{R_{\oplus}^2}{r^2}$	$\Phi_{\text{IR}} \approx 240, f_0 \approx 0.30, \alpha \approx 1.789$	2.5×10^{-11}	\neg
Asymmetric reflectivity	$\frac{1}{4} \frac{A}{M} \frac{\Phi_{\odot}}{c} \delta_a$	$\delta_a \simeq 0.015$	1.2×10^{-11}	\neg
Poynting-Robertson	$\frac{1}{4} \frac{A}{M} \frac{\Phi_{\odot}}{c} \frac{R_{\oplus}^2}{r^2} \frac{v}{c}$	$\Phi_{\odot} = 1360.8$	4.2×10^{-15}	1.9×10^{-14}
Thermal effect solar panels	$\frac{2}{3} \frac{\sigma}{c} \frac{A}{M} (\epsilon_1 T_1^4 - \epsilon_2 T_2^4)$	$\epsilon_1 \simeq \epsilon_2 \approx 0.8, T_1 \simeq 317, T_2 \simeq 318$		1.9×10^{-10}
Y-bias	Y_0 : empirical acceleration	Y_0		7.0×10^{-10}

TABLE III. LAGEOS II and Galileo FOC mean orbital elements, orbital period, cross section, mass, and area-to-mass ratio.

Element	Unit	Symbol	LAGEOS II	Galileo FOC
Semi-major axis	[km]	a	12162.07	29599.8
Eccentricity	[–]	e	0.0138	0.0000
Inclination	[deg]	i	52.66	56.00
Orbital period	[s]	P	13348.2	50680.9
Cross section	[m ²]	A	0.2827	13.2100
Mass	[kg]	M	405.380	709.138
Area/Mass	[m ² /kg]	A/M	6.97500×10^{-4}	1.86283×10^{-2}

(ILRS) [29]. The first column provides the physical effect responsible of the perturbation, while the second column gives the mathematical expression used to compute the order-of-magnitude of the corresponding acceleration. Finally, the third column provides the main parameters affecting the knowledge of the perturbation. LAGEOS II can also be considered a point of reference, since the best and most sophisticated models for the NGPs have been developed for its linear and rotational dynamics [50,115–117].

In Table III are shown, for each of the considered satellites, the orbital elements used to estimate the accelerations of Tables I and II (in particular the semimajor axis) with other parameters, as the area-to-mass ratio, useful for the estimate of the accelerations produced by the main NGPs.

For the normalized gravity field coefficients, $\tilde{C}_{\ell,m}$, those provided by the GGM05S model [118] from GRACE [119] data have been used. For the maximum degree, we considered $\ell = 12$, the truncation level (degree ℓ and order m) suggested by current IERS Conventions 2010 for the GNSS satellites [120] and the Earth’s gravitational coefficient GM_{\oplus} is still from IERS Conventions 2010. The main correction to the Newtonian equation of motion due to general relativity (GR) is also shown in Table I.

In the following, a few (but significant) considerations on the role of the NGPs on the Galileo satellites can be derived by the analysis of Table II together with previous considerations on their corresponding models.

- (1) The obvious consideration is the role played by the value of the satellite’s area-to-mass ratio. This immediately translates into a peak value for acceleration due to SRP of more than a factor of 40 greater for Galileo satellites than for LAGEOS II.
- (2) A second aspect is related to the greater distance from the Earth, which in part (apparently) compensates for the larger A/M of the Galileo, as can be seen from the effects due to the albedo and infrared radiation pressure compared to those on LAGEOS II.
- (3) The range of variability of the considered accelerations cover several orders of magnitude: three orders of magnitude in the case of the Galileo FOC satellites (from $\approx 10^{-7}$ m/s² down to $\approx 10^{-10}$ m/s²), and about

four orders of magnitude for LAGEOS II (from $\approx 10^{-9}$ m/s² down to $\approx 10^{-13}$ m/s²).

- (4) In the case of LAGEOS II several improved (and refined) models have been developed to account for the behavior of the perturbations down to a level of acceleration $\approx 10^{-12}$ m/s² [40,45,47,49,50,53,117,121]; conversely, in the case of the Galileo FOC current models account only down to about 10^{-10} m/s², but with several drawbacks.
- (5) Because of the complex shape of the Galileo FOC and the additional fact that they are active satellites, also the uncertainties of the parameters that enter in their modeling are (in general) larger with respect to those of LAGEOS II (see next subsection).

Therefore, the overall modeling is worse in the case of the Galileo satellites with respect to LAGEOS-like satellites; this also explains why we used the term “apparently” in the point 2. above. Indeed, from all the literature available on GNSS satellites it is evident that a number of different NGPs are competing in the acceleration range between 10^{-9} m/s² and 10^{-10} m/s² [19,20,122]. This acceleration interval represents the granularity of the NGPs, within which it is difficult to clearly and univocally separate the various effects that make it up. Therefore, we can affirm that the actual “noise level” of the current NGPs models is around 10^{-10} m/s². This level of uncertainty can also be simply obtained from Table II considering the uncertainty of the main parameter that characterizes each perturbative acceleration. These aspects will be further discussed in the next subsection.

We finally conclude with a brief discussion on the use of the empirical terms, the outstanding example in the field of GNSS is represented by the so-called Y-bias, see Table II. We have already highlighted the positive role of empirical terms in absorbing unknown effects at the price, however, of losing the physical content of some perturbative effects. In the end, in the GNSS literature, it seems that the main objective is to reduce the POD residuals of these satellites by exploiting the modeling of the direct SRP, currently with a BW, and absorbing the other effects, as much as possible, through the *ad hoc* introduction of empirical terms, which however have the primary objective of absorbing the

1098 unmodeled part of the SRP which is not taken into account
 1099 by the BW model (see [20]).

1100 This aspect is clearly expressed in the paper by [17]: “In
 1101 our case, the interest is not to study the effects of SRP on
 1102 the orbits, but rather to fit the measurements of the orbits
 1103 (GPS tracking data) with a model capable of compensat-
 1104 ing the SRP acting on the satellites, which is assumed to
 1105 be the major error source affecting the GPS satellite orbits.
 1106 By doing this an improvement in the orbits themselves is
 1107 also expected.”

1108 The last sentence, “*By doing this an improvement in the*
 1109 *orbits themselves is also expected,*” is in principle correct
 1110 because, in the end, thanks to the empirical terms, it is
 1111 possible to reduce the orbit residuals, and this is positive for
 1112 Positioning, however, the sentence is questionable for other
 1113 applications of GNSS satellites, such as for geophysics and
 1114 fundamental physics.

1115 As a methodological guideline, our interest is, contrary
 1116 to that of [17], to understand the effects of the SRP on the
 1117 orbital elements of navigation satellites and, in particular,
 1118 for the Galileo ones. On these aspects, see the accompany-
 1119 ing article [123], hereafter Paper II. For these reasons, we
 1120 believe that a greater effort must be made in modeling the
 1121 perturbative effects of nongravitational origin, in order to
 1122 reduce their current limits. This will also help to establish
 1123 the characteristics of an onboard accelerometer that can
 1124 match, complement and overcome the performance of the
 1125 models themselves within a POD.

1126 **A. NGPs intrinsic uncertainties**

1127 In this section, we will try to analyze the intrinsic
 1128 precision of the models, without taking into account their
 1129 precision/accuracy within an analysis based on the reduc-
 1130 tion of observational data, i.e., within a POD, with the
 1131 consequent possible estimate of some parameters of the
 1132 models themselves and/or of any empirical terms. We will
 1133 limit this analysis to nongravitational perturbations. In fact,
 1134 in the case of gravitational perturbations, the accelerations
 1135 linked to the uncertainties of the various coefficients that

characterize them—starting from that of the terrestrial 1136
 quadrupole which produces the greatest acceleration, 1137
 approximately $8 \times 10^{-12} \text{ m/s}^2$ —are much smaller than 1138
 those attributable, for example, to thermal effects as 1139
 indicated in Table II. 1140

Based on the results obtained for the order of magnitude 1141
 of the accelerations estimated for the various NGPs 1142
 acting on a Galileo satellite, see Table II and the relative 1143
 discussion, we will limit our analysis on the precision of the 1144
 models to effects with accelerations $\geq 10^{-10} \text{ m/s}^2$. Of 1145
 course, the two most important effects to be considered 1146
 are the perturbations due to the direct and indirect SRP 1147
 effects (i.e., the albedo). 1148

In Table IV are shown the estimates, in order of 1149
 magnitude, of the precision for some of the models of 1150
 Table II. In column 2, the main parameters limiting the 1151
 precision of the perturbative effects of column 1 are 1152
 highlighted. Column 3 provides an estimate of the relative 1153
 uncertainty of said parameters. This is based on the 1154
 knowledge that we currently have of the parameters that 1155
 characterize the models or that we will be able to achieve 1156
 in the case of a box-wing model that is more performing 1157
 (i.e a R-BW) than the current ones based on the knowledge 1158
 of the Galileo FOC metadata (i.e., S-BW). 1159

The relative uncertainties allow us to rescale the amplitude 1160
 of the accelerations in Table II and estimate their precision 1161
 for the effects considered and for each satellite: LAGEOS II 1162
 in column 4 and a Galileo FOC, modeled with a S-BW in 1163
 column 5 and with a R-BW in column 6. As for the relative 1164
 error, when several parameters, not correlated with each 1165
 other, contribute to its estimate, the error is estimated on the 1166
 basis of their quadratic sum, that is in a root-sum-squared 1167
 fashion. In general, in a measurement process, relative 1168
 error is an indication of measurement accuracy only in 1169
 the absence of systematic errors. When there are systematic 1170
 errors, relative error is only an indication of the precision of a 1171
 measurement and not its accuracy. 1172

In the current simplified context of model error analysis, 1173
 we will not consider the actual accuracy of models, in the 1174

TABLE IV. Intrinsic uncertainties of the models and corresponding uncertainties in acceleration. The uncertainties highlighted in column 3 were estimated through the quadratic sum of the errors of the parameters reported in column 2. The three values of this uncertainty refer, respectively, to LAGEOS II, to a Galileo approximated by a simplified box-wing (S-BW) model and to a Galileo approximated by a reliable box-wing (R-BW) model. Column 5 provides an estimate of the error in acceleration in the case of a Galileo FOC modeled with a S-BW model based on current Galileo metadata information. Conversely, column 6 provides an estimate of the error in the hypothesis of a Galileo FOC modeled with a R-BW model constructed with more detailed information than that of the Galileo metadata. A R-BW model must be considered a preliminary FEM.

Physical effect	Parameter	Relative uncertainty	LAGEOS II	S-BW	R-BW
Direct SRP	$C_R, \frac{A}{M}, \Phi_{\odot}$, Optical coefficients	0.02/0.30/0.05	6.4×10^{-11}	3.0×10^{-8}	5.0×10^{-9}
Earth’s albedo	$\frac{A}{M}, \Phi_{\odot}, A_{\oplus}$, Optical coefficients	0.30/0.43/0.30	3.9×10^{-11}	3.0×10^{-10}	2.1×10^{-10}
Earth’s infrared radiation	$\frac{A}{M}, \Phi_{\text{IR}}$, Optical coefficients	0.1/0.1/0.1	1.5×10^{-11}	1.1×10^{-10}	1.1×10^{-10}
Power from antennas	P, M, ξ	/0.06/0.02		7.2×10^{-11}	2.4×10^{-11}
Thermal effect solar panels	$\frac{A}{M}, \epsilon, T$	/0.06/0.03		1.1×10^{-11}	5.7×10^{-12}
Y-bias	Y_0	/0.086/0.043		6.0×10^{-11}	3.0×10^{-11}

sense of estimating their systematic errors. This aspect will be addressed, as far as possible, in the context of a precise determination of the orbit in a future work.

The following preliminary considerations can be drawn from the analysis of Table IV:

- (1) It is interesting to note that in the case of the Galileos, when the noise threshold of the NGPs ($\approx 10^{-10}$ m/s²) and the *a priori* errors of the model parameters are considered, the perturbations to be effectively taken into account are restricted to the first three in magnitude: direct SRP, Earth’s albedo and infrared radiation.
- (2) However, only the uncertainty of the SRP acceleration is well above the “*noise level*” of the NGPs that characterize the Galileo satellites, whereas the acceleration uncertainty of both the terrestrial albedo and infrared radiation pressure falls within this “*noise level*.”
- (3) This means that the acceleration uncertainties in the models of albedo and infrared radiation are of the order of the perturbative effects produced by other (smaller) nonconservative forces, such as thermal effects.
- (4) Therefore, several different nongravitational forces combine to create a sort of limbo within which, up to now, it is not possible to clearly separate the different perturbative effects in order to improve the global dynamic model of the orbit of the Galileo satellites, and of GNSS satellites in general.
- (5) A better understanding of thermal effects and their inclusion in the dynamic model is yet to come; an indispensable prerequisite in this direction remains a significant improvement of the overall model, solar and terrestrial, for the effects deriving from the radiation pressure.
- (6) On the contrary, in the case of LAGEOS II, the acceleration uncertainties are between 1 and 2 orders of magnitude greater than the noise level of its dynamic model for NGPs, consequently their effects can be well distinguished from those of other smaller perturbations.
- (7) A step toward an R-BW model, midway between an S-BW model and an FEM, will probably only allow for model improvement for direct SRP, but improvements in albedo and terrestrial infrared radiation will likely not be significant.

As previously highlighted, here we analyzed the inherent precision of NGPs models and not their posterior accuracy once included in the POD process. Of course, during the POD, improvements are present thanks to the estimation and adjustment of the model parameters.

The results we have derived are obviously a function of the overall relative error we have assumed for each of the models considered in Table IV. The relative uncertainties indicated in the table are based on estimates made for the

respective parameters in independent analyzes, and obviously cannot be considered completely reliable, also thanks to the currently scarce information on the characteristics of the Galileo FOC satellites. Nevertheless, even assuming a factor of 2 or 3 of discrepancy with respect to more truthful values, the quality and substance of the previous arguments do not fail.

A further aspect to consider when discussing the results shown in Table IV is related to the spectral content of the perturbations considered. In fact, in the case of perturbations characterized by a different spectral content, these are in principle more easily separable even if of comparable amplitudes. It is also important to underline that, once a given perturbation is fixed, the spectrum associated with it depends precisely on the goodness of the model used to include it in the dynamic model of the orbit: the spectrum obtained with a box-wing model will be richer in details than the one which is obtained with a cannon ball, but less detailed than the spectrum that can be obtained with a FEM for the spacecraft. For the details of the spectral content we obtained with our box-wing model we refer to Paper II.

Finally, an aspect to consider concerns the difference between periodic perturbations and constant or slowly variable perturbations over time. The latter can be absorbed by an empirical term that can make up for the lack of an adequate model. This is the case of the Y-bias acceleration, or the case of the acceleration due to the antennas, which is mainly directed radially outward from the Earth. Conversely, in the case of periodic effects, the advantage of a reliable model (or of an accelerometer) is indisputable. This is the case of the direct solar radiation pressure. In this case, see Table IV, we can see the clear advantage of a reliable model in determining more precisely the amplitude of periodic effects, at orbital frequency and its higher multiples [124].

V. TOWARDS THE FEM: 3D-CAD AND PRELIMINARY BOX-WING

As previously anticipated, the Metadata provided by ESA on the characteristics of Galileo satellites, although in general they are useful and rich in multiple information, are not sufficiently detailed for the construction of a complex model for the structure of a Galileo FOC type satellite, as in the case of a FEM.

Tables V and VI, adapted from ESA Metadata, show the available information regarding the dimensions of the box

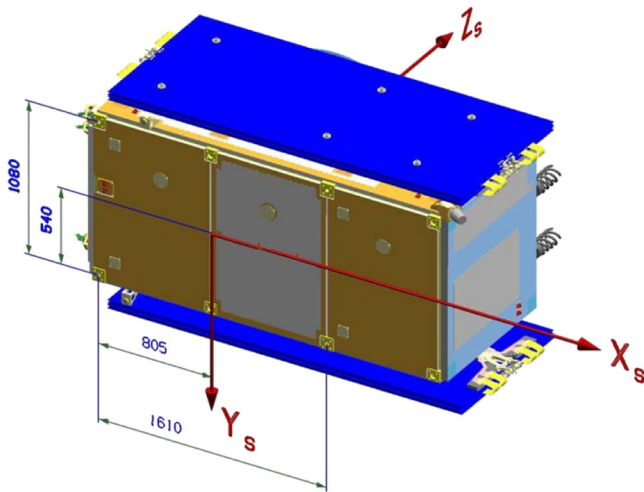
TABLE V. Dimensions and surface areas of the box of Galileo FOC satellites from ESA metadata.

	Dimensions [m]		Surface areas [m ²]	
	ΔX	ΔY	±X panel	±Y panel
	2.530	1.200	1.320	2.783
	1.100		±Z panel	3.036

TABLE VI. Surfaces of the satellite with their (approximated) materials, corresponding area and optical coefficients from ESA metadata. The physical meaning of these optical coefficients was introduced in the previous Sec. III B 4 and should be understood as average values for the coefficients of the materials in the visible part of the electromagnetic spectrum.

Surface	Material	Area m ²	α	ρ	δ	
Box	+X	A	0.440	0.93	0.00	0.07
		C	0.880	0.08	0.73	0.19
	-X	A	1.320	0.93	0.00	0.07
	+Y	A	1.129	0.93	0.00	0.07
		C	1.654	0.08	0.73	0.19
	-Y	A	1.244	0.93	0.00	0.07
		C	1.539	0.08	0.73	0.19
	+Z	A	1.053	0.93	0.00	0.07
	B	1.969	0.57	0.22	0.21	
	A	2.077	0.93	0.00	0.07	
	C	0.959	0.08	0.73	0.19	
Wing	+SA	E	3.880	0.92	0.08	0.00
		D	1.530	0.90	0.10	0.00
	-SA	E	3.880	0.92	0.08	0.00
		D	1.530	0.90	0.10	0.00

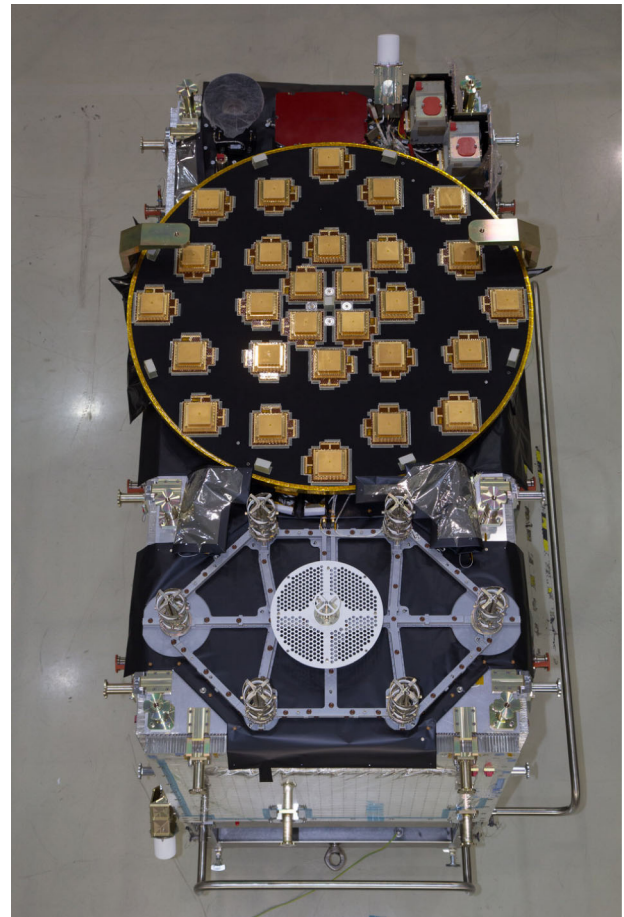
1274 spacecraft and the average optical coefficients for the box
 1275 panels and for the solar array (SA) of the Wings. The
 1276 dimensions are provided with respect to the mechanical
 1277 reference frame (MRF) of the spacecraft, see Fig. 1, while
 1278 the complex elements located on the surfaces of the all
 1279 spacecraft, especially of the box, are approximated by a few
 1280 materials.



F1:1 FIG. 1. Galileo FOC spacecraft: the mechanical reference
 F1:2 frame. The MRF s aligned with the main body axes and originates
 F1:3 in the separation plane of dispenser and satellite in the exact
 F1:4 middle of the four I/F point center lines. The $+Z_s$ -axis is normal
 F1:5 to the separation plane and points toward the L-band navigation
 F1:6 antenna. The $+X_s$ -axis is normal to the clock panel and points
 F1:7 toward the clock panel. The $+Y_s$ -axis completes the right-handed
 F1:8 orthogonal system. Courtesy of ESA from Galileo metadata.

1281 As we can see from Table VI, five different materials
 1282 (letters A–E) have been introduced as a very rough
 1283 approximation of the real spacecraft. This is evident if
 1284 we consider the surface $+Z$, that is, the one facing the
 1285 Earth. This surface in the Metadata was considered to
 1286 consist of only two materials, A and B, whose combined
 1287 characteristics are not comparable with those of the real
 1288 components of the surface. In fact, the real surface (see
 1289 Fig. 2) is equipped with a set of antennas (e.g. L-band
 1290 SAR and C-band) [125], corner cube retroreflectors
 1291 (CCR) and Earth sensors, just to mark the most evident
 1292 differences, which have very different optical character-
 1293 istics from each other and also compared to those of the
 1294 same metadata.

1295 However, as shown in Fig. 3 for the flight version of the
 1296 spacecraft, both the L-band antenna and the exagonal
 1297 surface occupied by the SAR antennas are covered by a
 1298 Mylar sheet coated with Silver and Beryllium. This means
 1299 that for these elements, the mylar optical properties must be
 1300 considered in the modeling process. Therefore, considering
 1301 the properties of the mylar and not those of the L-band
 1302 antenna, represents one of the necessary steps toward the
 1303 construction of a satellite model more relevant to reality



F2:1 FIG. 2. Galileo FOC spacecraft: photo of the $+Z$ panel.
 F2:2 Courtesy of ESA.



F3:1 FIG. 3. Galileo FOC spacecraft: photo of four satellites at OHB
 F3:2 in Bremen. Courtesy of ESA.

1304 than a simple box-wing based on Galileo metadata. In the
 1305 case of the SAR antennas, three different materials have
 1306 to be considered: (i) the mentioned mylar sheet for the
 1307 exagonal plate, (ii) Aluminium (probably anodized) for the
 1308 six radiating elements (the elicoidal antennas), and (iii) a
 1309 white paint for the circular plate (i.e., the subreflector
 1310 ground plate).

1311 It should be noted that the nonsmooth surface of the
 1312 mylar will complicate the correct application of the ray-
 1313 tracing technique for these elements, giving for example a
 1314 partly random character to the specular reflection.

1315 Therefore, if ESA (or OHB, which built the satellites)
 1316 does not release further updates of the optical properties
 1317 for the different surface elements in the future, and with
 1318 sufficient detail to build a FEM (or at least a R-BW model),
 1319 it will be necessary to proceed with *ad hoc* hypotheses, the
 1320 most plausible from the physical point of view, to fix the
 1321 values for the physical properties of the various materials.
 1322 In this case, the results of the PODs will give us a rough
 1323 indication (necessarily more qualitative than quantitative)
 1324 on the validity of our *a priori* hypotheses, for example on
 1325 the basis of the statistic and distribution of the post-fit
 1326 residuals obtained.

1327 In the following sections, we present the 3D model and a
 1328 box-wing model for the spacecraft that we built for the
 1329 forthcoming activities of G4S_2.0.

1330 A. 3D-CAD model with SolidWorks

1331 Since the information contained on the metadata of the
 1332 Galileo satellites is very scarce, all the dimensions neces-
 1333 sary to build a 3D model of the satellite have been obtained
 1334 indirectly, such as the distances between the different
 1335 elements of the surfaces and their location on the same,
 1336 through the numerous photographs of the Galileo FOC
 1337 satellites available on the web.

1338 In fact, we reconstructed the size and position of the
 1339 different parts of the satellite based on the large amount
 1340 of photos, taken from many points of view, representing
 1341 the satellite during assembly and ground tests by ESA.

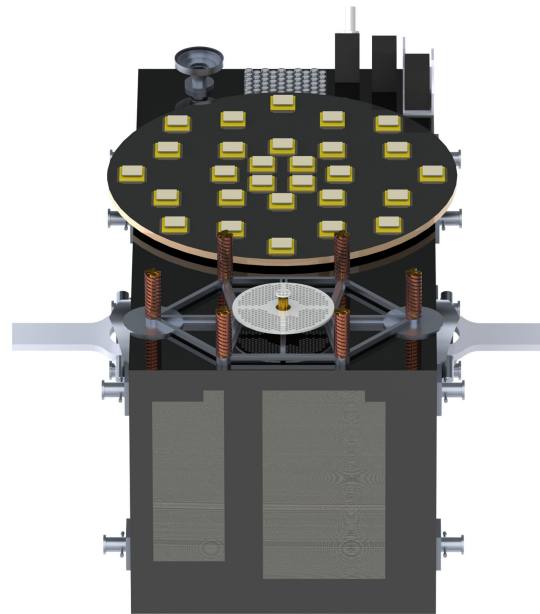
1342 A very powerful tool for this process was the SketchUp
 1343 program ([126]).

1344 Using this program we have first drawn a parallelepiped
 1345 having the dimensions reported in the Galileo metadata for
 1346 the box, see Table V. Then, many photos representing the
 1347 different parts of the satellite have been matched to this
 1348 drawing. The program allows to modify the representation
 1349 of the 3D model drawn in it, changing the point of view and
 1350 the focal length. Consequently, these parameters have been
 1351 modified trying to perfectly superimpose the drawing on
 1352 the photo used as background.

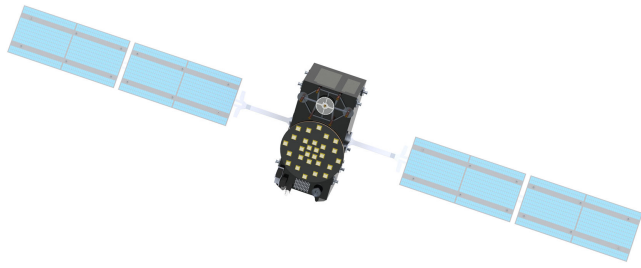
1353 The program also allows you to “glue” the correspond-
 1354 ing parts of the photo to the sides of the 3D solid. After
 1355 pairing, if you choose a different perspective to view the 3D
 1356 box, the part of the photo changes along with the side it is
 1357 pasted on. By choosing the most convenient perspective,
 1358 using the program’s “measure” tool, it is possible to obtain
 1359 the positions of the different components on each face, as
 1360 said. Of course, the operation is much less affected by error
 1361 the more the photo used is taken from a direction normal to
 1362 the surface. Finally, the different measurements obtained
 1363 with this procedure were used to draw a 3D model in a
 1364 CAD (Computer Aided Design): SolidWorks ([127]) was
 1365 used [128].

1366 This is shown in Figs. 4 and 5 for our current 3D-CAD
 1367 model of the Galileo FOC spacecraft. From these figures it
 1368 is possible to detect the high degree of detail of the surfaces
 1369 achieved in our model, as can be seen from their com-
 1370 parison with the photo of the satellite shown in Fig. 2.

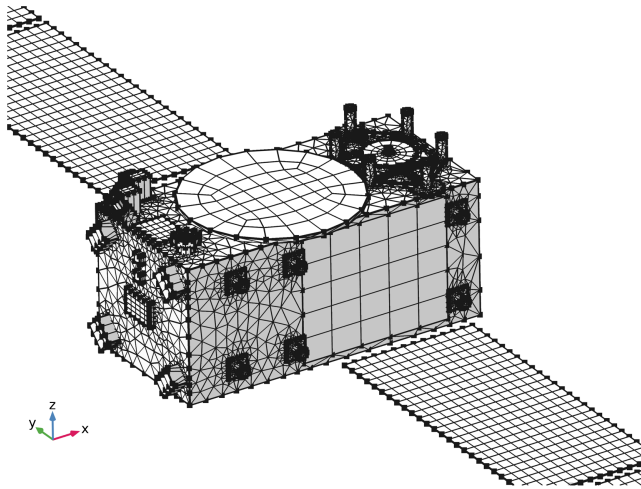
1371 Naturally, to proceed with the application of ray-tracing,
 1372 the different surfaces and the different elements of the 3D
 1373 model must be discretized to a level of detail suitable for



F4:1 FIG. 4. 3D-CAD model of a Galileo FOC spacecraft. The +Z
 F4:2 and +X surfaces are shown.



F5:1 FIG. 5. 3D-CAD model of a Galileo FOC spacecraft. The +Z
F5:2 and +X surfaces are shown with the solar panels.



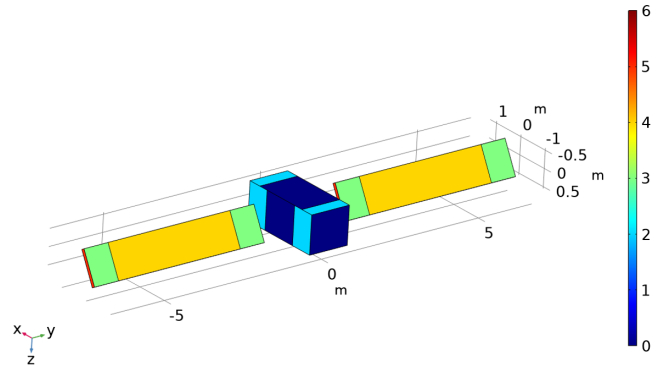
F6:1 FIG. 6. A very preliminary partial mesh of the 3D-CAD model
F6:2 of a Galileo FOC spacecraft. The +Z, -X and -Y surfaces
F6:3 are shown with part of the solar panels.

1374 them by means of an appropriate mesh. In Fig. 6, it is
1375 shown a preliminary rough example of mesh produced with
1376 COMSOL [129].

B. S-BW model and COMSOL

1378 In Sec. III A we underlined the difficulties that can be
1379 encountered to fully characterize a FEM of the Galileo
1380 FOC spacecraft from the physical point of view. In case
1381 these difficulties will be not overcome, due to lack of
1382 necessary information, we will focus on developing a
1383 superior box-wing which we have already called in
1384 Sec. III B 5 as a reliable box-wing (R-BW) model. This
1385 R-BW model will have to be characterized by the greatest
1386 possible number of information for the different surfaces
1387 and the different elements that compose them.

1388 A ray tracing algorithm is being developed in MATLAB
1389 code and while we are currently finalizing the code in
1390 MATLAB to test them on the FEM or on the R-BW of the
1391 Galileo FOC satellites, we have proceeded with the start
1392 of a preliminary activity on our box-wing model of the
1393 satellite—the S-BW model built with ESA metadata—
1394 embedded within the COMSOL MultiPhysics [129] tools.



F7:1 FIG. 7. COMSOL representation of the S-BW model for a
F7:2 Galileo FOC spacecraft based on ESA Metadata. The different
F7:3 colors reflect the materials in Table VI with the corresponding
F7:4 optical coefficients.

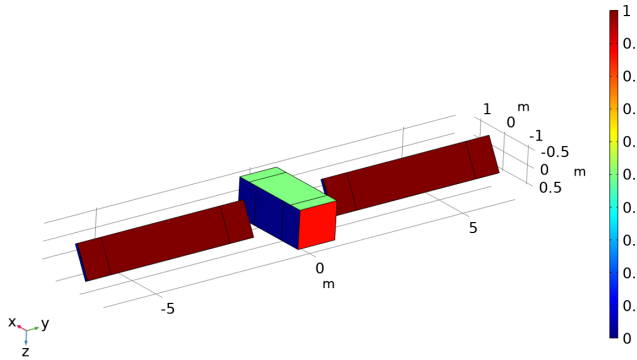
1395 Figure 7 shows the COMSOL version of the S-BW
1396 model used in our simulations. The box-wing is drawn
1397 respecting the dimensions and areas described in Table V,
1398 while the colors correspond to the materials (and corre-
1399 sponding areas) described in Table VI. The reference
1400 system corresponds to the MRF previously introduced
1401 in Fig. 1.

1402 The simulation was parameterized with respect to an
1403 angle ψ ranging between 0° and 180° , which is defined as
1404 the angle of the +X vector referred to the box around +Y,
1405 from its initial position -Z (corresponding to $\psi = 0^\circ$) to its
1406 final position +Z (corresponding to $\psi = 180^\circ$). The unit
1407 vector \hat{e}_D , that identifies the direction of the Sun, also
1408 rotates following ψ . Solar panels have always been
1409 considered orthogonal to the direction of the Sun and
1410 therefore not rotating with the box of the satellite.

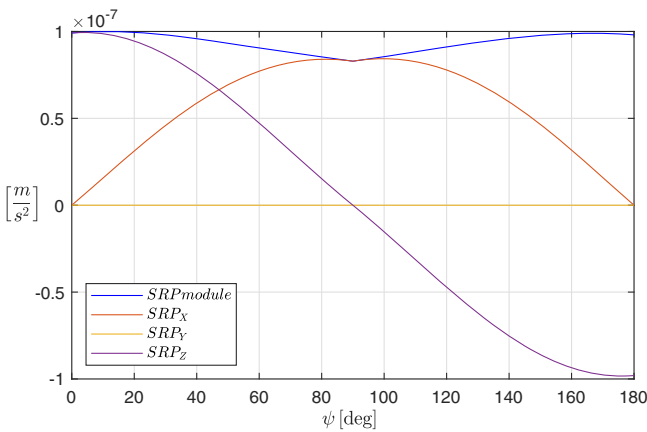
1411 The *view factors* were calculated by COMSOL using the
1412 physics of its “surface-to-surface radiation” module [130].
1413 Not using at the moment the ray-tracing technique of
1414 COMSOL, that of the calculation of the *view factors* is an
1415 expedient to determine the quantity of solar radiation that
1416 radiates each surface of the satellite in order to be able
1417 to determine the corresponding acceleration according to
1418 Eq. (5). Figure 8 shows the values of the *view factors* (color
1419 bar) when $\psi = 60^\circ$.

1420 Once the accelerations acting on each face of the S-BW
1421 have been calculated, these are projected into the body
1422 frame of the spacecraft identified by the MRF. These
1423 accelerations, and the corresponding absolute value, are
1424 plotted in Fig. 9 as a function of ψ . Obviously the
1425 acceleration along the Y-axis is always zero in this ideal
1426 situation (i.e., with the solar panels always orthogonal to
1427 the Sun direction) and furthermore the acceleration due to
1428 the wings is constant.

1429 We then proceeded to compare the solution for the
1430 accelerations produced by direct solar radiation using the
1431 COMSOL model for the S-BW with a numerical solution
1432 obtained with a specially developed MATLAB numerical



F8:1 FIG. 8. View factors for the S-BW model in COMSOL for
 F8:2 $\psi = 60^\circ$. For clarity, when $\psi = 0^\circ$ the solar rays are orthogonal to
 F8:3 the $-Z$ face of the satellite, when $\psi = 90^\circ$ the solar rays are
 F8:4 orthogonal to the $-X$ face, and finally when $\psi = 180^\circ$ the solar
 F8:5 rays are orthogonal to the $+Z$ face.



F9:1 FIG. 9. Direct SRP acceleration in the body frame identified by
 F9:2 the MRF. The components and the absolute value (blue line) of
 F9:3 the acceleration due to the Sun radiation pressure are plotted as a
 F9:4 function of the rotating angle ψ .

1433 code ([131]). As already specified, this second model
 1434 and the corresponding solutions are described in detail
 1435 in Paper II in the case of the direct SRP. In particular we:

- 1436 (1) Verified the consistency of the reference systems
 1437 used.
- 1438 (2) Verified the consistency of the results on the single
 1439 surfaces of the satellite.
- 1440 (3) Compared the results over a 500 days simulation.

1441 Figure 10 shows the comparison for the module of the
 1442 acceleration produced by the SRP acting on the S-BW
 1443 obtained with the COMSOL model and with the MATLAB
 1444 numerical code. Since in the model developed in MATLAB
 1445 the accelerations are calculated as a function of time, first of
 1446 all the COMSOL vs angle solution was transformed into a
 1447 COMSOL vs time solution. Therefore, a time vector has
 1448 been constructed which interpolates the COMSOL solution
 1449 vs angle for each angle vs time. For simplicity, in this
 1450 test the Earth-Sun distance was considered fixed at 1

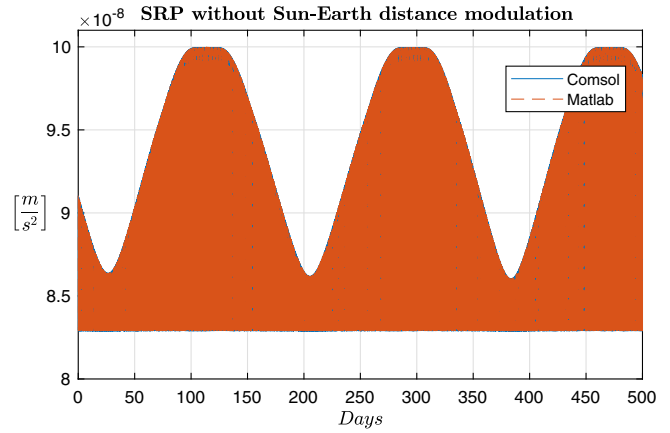


FIG. 10. Absolute value of the direct SRP acceleration on the S-BW model obtained with COMSOL (blue line), as a function of time, compared to the same acceleration obtained with the S-BW model implemented with MATLAB (brown line).
 F10:1
 F10:2
 F10:3
 F10:4

astronomical unit, as it does not affect the quality of the comparison.
 1451
 1452

As can be seen, the two solutions are practically coincident. The only significant difference lies with the different attitude law of the spacecraft in the two cases. In the case of COMSOL, a nominal attitude was always assumed with the surface of the solar panels orthogonal to the solar radiation. In the case of the numerical code, the attitude variation of the satellite during the eclipses season was taken into account according to the attitude variation described in the ESA Metadata. This is shown in Fig. 11, where the difference between the two accelerations is plotted.
 1453
 1454
 1455
 1456
 1457
 1458
 1459
 1460
 1461
 1462

The three minimum in acceleration, lasting about 10 days each, characterize the eclipse season—that is, when the Sun is relatively low on the satellite’s orbital plane—with a periodicity of about 175 days. The residual acceleration that can be seen in the figure, which is characterized by an
 1463
 1464
 1465
 1466
 1467

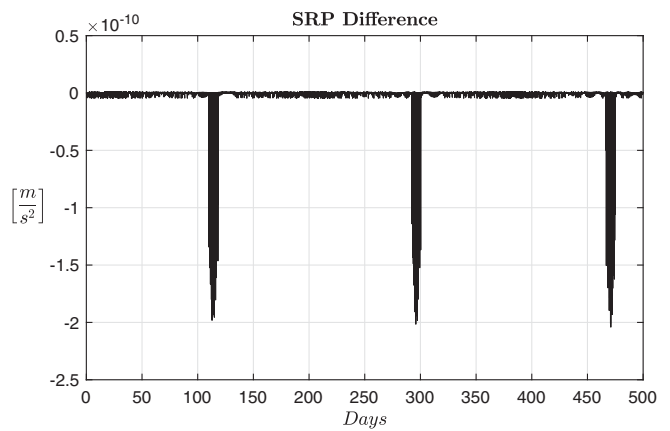
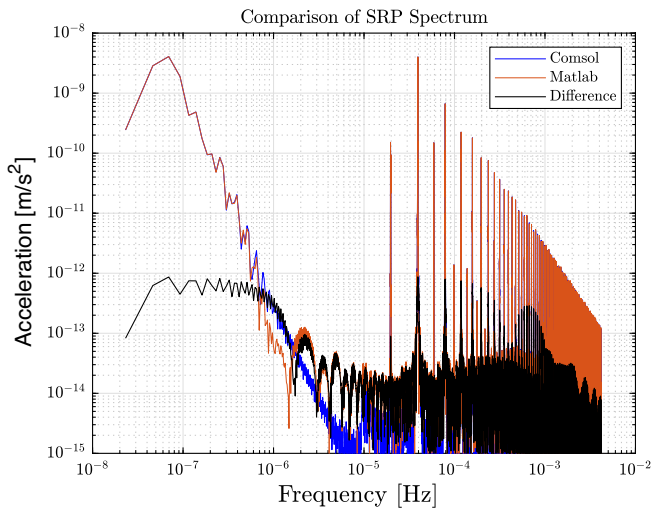


FIG. 11. Difference in the absolute value of the direct SRP acceleration obtained with the MATLAB model with the corresponding acceleration obtained with COMSOL.
 F11:1
 F11:2
 F11:3



F12:1 FIG. 12. Fast Fourier transform of the absolute value of the SRP
 F12:2 as obtained with COMSOL (blue) and with the numerical code
 F12:3 (orange) and of their difference (black).

1468 average value of about $-5 \times 10^{-14} \text{ m/s}^2$ and a peak-to-
 1469 peak variation of about $5 \times 10^{-12} \text{ m/s}^2$, is actually a
 1470 numerical artifact of the current integration process in
 1471 MATLAB. In fact, it does not in itself constitute a problem:
 1472 on the one hand it can be canceled by decreasing the
 1473 integration step in the model developed in MATLAB (cur-
 1474 rently 120 s), while on the other hand we are interested in
 1475 reaching a level of precision in the modeling of the
 1476 nongravitational accelerations down to the order of
 1477 10^{-10} m/s^2 , as the one reached during the eclipse season,
 1478 i.e., two order-of-magnitude larger than the peak-to-peak
 1479 variation in Fig. 11. Figure 12 provides the representation
 1480 of Figs. 10 and 11 in the frequency domain. As can be
 1481 seen, the lines at the orbital frequency of the satellite
 1482 ($f_{\text{orb}} \simeq 1.97 \times 10^{-5} \text{ Hz}$) and at its higher integer multiples
 1483 are clearly visible both in the case of the COMSOL model
 1484 and in the numerical one obtained with MATLAB. In the
 1485 case of the spectrum of the difference between the two
 1486 models, the amplitudes of the lines are of the order
 1487 of $\approx 10^{-12} \text{ m/s}^2$.

1488 The next steps in the use of COMSOL concern the
 1489 implementation of the rotation of the satellite around the
 1490 yaw axis, i.e., around the Earth-satellite radial direction and
 1491 a first application of the MATLAB ray-tracing algorithms to a
 1492 simplified 3D model of the spacecraft with respect to the
 1493 one presented in Sec. VA.

1494 **VI. CONCLUSIONS AND RECOMMENDATIONS**

1495 In this work we introduced some of the activities
 1496 currently in progress at IAPS/INAF within the G4S_2.0
 1497 project. These activities focus on the study of noncon-
 1498 servative forces on the Galileo FOC satellites and the
 1499 consequent development of an appropriate model of the
 1500 real satellite in order to account for their perturbative

1501 effects. In this regard, the main challenge is to significantly
 1502 improve, compared to the state of the art, the modeling of
 1503 the orbital effects related to the direct solar radiation
 1504 pressure, indeed the largest nongravitational perturbation
 1505 on GNSS satellites. This is motivated by the fact, as
 1506 already highlighted above, that some of the ambitious
 1507 goals of G4S_2.0—such as an improvement in the
 1508 accuracy of the gravitational redshift measurement or
 1509 the measurement of relativistic precessions on the orbits
 1510 of the GSAT-0201 and GSAT-0202 satellites—require an
 1511 improvement of the dynamic model of the orbits of the
 1512 Galileo FOC satellites, starting with the model of pertur-
 1513 bations of nongravitational origin.

1514 In order to fully carry out this task, the state of the art
 1515 was then evaluated (see Secs. II and III) with regard to the
 1516 main models developed so far in the literature to take into
 1517 account the perturbative effects produced by the direct solar
 1518 radiation pressure and by other (much smaller) noncon-
 1519 servative forces that act on the Galileo FOC satellites and
 1520 on the GNSS satellites in general. This allowed us to feature
 1521 the types and peculiarities of the different models, high-
 1522 lighting their advantages and disadvantages, as well as their
 1523 actual degree of implementation in the orbit determination
 1524 softwares. For example, the models based on a satellite
 1525 FEM, although developed by several authors in the
 1526 literature, do not seem to be used by the different GNSS
 1527 analysis centers, generally preferring a simple box-wing
 1528 model with the concomitant estimate of a certain number of
 1529 empirical accelerations. This is probably linked both to the
 1530 difficulty of including the FEM of the spacecraft in the
 1531 PODs processes with the consequent application of the ray-
 1532 tracing technique to it, and to an actual lack of an accurate
 1533 knowledge of the “fine structure” of the satellites, starting
 1534 with their optical properties and their consequent evolution
 1535 (say degradation) with the passage of time. As described in
 1536 the previous sections, we are interested in developing a
 1537 *superior* model of the satellite, possibly a model that comes
 1538 as close as possible to a FEM, to be used in our PODs in the
 1539 field of fundamental physics.

1540 A significant aspect, we believe, of the work carried out
 1541 in this first phase, was to quantify not only the orders of
 1542 magnitude of the various nongravitational perturbations
 1543 involved, an aspect already addressed in the literature but
 1544 probably not with the extension and in-depth analysis we
 1545 presented, but also to critically evaluate the intrinsic
 1546 uncertainties of the current models and their possible
 1547 improvement with more performing models (see Sec. IV).
 1548 This has allowed us to establish that the current *intrinsic*
 1549 *noise level* of the nongravitational accelerations that the
 1550 models provide, currently in the $10^{-9} \div 10^{-10} \text{ m/s}^2$ range,
 1551 may be reduced in the future down to 10^{-10} m/s^2 only if a
 1552 great effort at the satellite knowledge level will be done by
 1553 the space agencies and the industries in charge of the
 1554 spacecraft construction and assembly, but it is unlikely that
 1555 it will be reduced further. We therefore think that it is

1556 fundamental for the new future constellations of GNSS
 1557 satellites that the various space agencies involve the
 1558 industry in a series of ground tests to finely characterize
 1559 all the elements and surfaces of the satellites, in order to
 1560 define all the useful physical properties to the development
 1561 of new perturbative models for accelerations of nongravita-
 1562 tional origin. Of course, once all this technical information
 1563 has been determined, it will necessarily need to be shared
 1564 with the scientific community.

1565 Naturally, and this has been pointed out previously, here
 1566 we are considering the intrinsic precision, *per se*, of the
 1567 models, and not that which is obtained *a posteriori* thanks
 1568 to the orbital determination process with the concomitant
 1569 possible estimation of some of the parameters that
 1570 characterize a certain perturbative model. For example,
 1571 a model would be very useful for the knowledge of the
 1572 temperature distribution on the surface of the satellite and
 1573 inside it, in the two extreme cases in which the satellite is
 1574 fully illuminated by the Sun and in the case of eclipses. In
 1575 this case, the characterization of the thermal inertia of the
 1576 different elements is of primary importance. In this regard,
 1577 it was also underlined how an accelerometer, with appro-
 1578 priate sensitivity and measurement band, can provide a
 1579 qualitative leap in this context thanks to the direct
 1580 measurement of nongravitational accelerations and the
 1581 process of their integration. This is in fact one of the
 1582 objectives of the G4S_2.0 project, namely the develop-
 1583 ment of an accelerometer for a future generation of
 1584 Galileo satellites, the readings of which would in any
 1585 case complement the predictions provided by the models
 1586 without replacing them.

1587 In Sec. V, we introduced the two models we developed
 1588 so far the Galileo FOC spacecraft. The first is a 3D model
 1589 of the satellite. As explained in Secs. III and VA, the final
 1590 purpose is to best characterize the different elements of the
 1591 satellite to create an appropriate mesh of the satellite and
 1592 apply the ray-tracing technique on top of it. If this is
 1593 successful, we will have a FEM of a Galileo FOC which
 1594 will allow us first of all to greatly improve the modeling of
 1595 the solar radiation pressure effects. In fact, as has been
 1596 explained, the construction of a 3D-CAD of the satellite is
 1597 the main prerequisite for the implementation of a satellite
 1598 FEM. The most difficult part then lies in the detailed
 1599 knowledge of the physical properties for the different
 1600 elements and, finally, in the implementation of an optimal
 1601 ray-tracing technique. These aspects will be addressed in
 1602 the project's future activities.

1603 The second satellite model we have built is a simplified
 1604 box-wing (S-BW). This provides us with a basic model on
 1605 which to evaluate future improvements on the satellite's
 1606 model (i.e., toward the FEM) as our knowledge on its
 1607 intrinsic physical characteristics (optical, thermal, etc.)
 1608 increases. The first applications of the S-BW are described
 1609 in the paper accompanying the present in this same issue.

We will use, as one of the possible indicators to evaluate
 the goodness of our more detailed satellite models, the
 results of the PODs that we will obtain with the s/w
 GEODYN II [132], evaluating the range residuals (with
 their statistics) but also the orbital residuals [133] of the
 considered satellites. An important further application of
 the box-wing model is its use within COMSOL as a first
 experimental test bed for ray-tracing applications. The
 preliminary applications of the S-BW in this perspective
 have been described in Sec. VB, and constitute a sort of
 “calibration” of the S-BW in COMSOL for the continu-
 ation of these activities.

Finally, an aspect to be reiterated further, directly linked
 to what we have defined as the *intrinsic noise level* of the
 nongravitational accelerations, concerns the perturbative
 effects of thermal origin (Secs. II and IV). These can be
 taken into due consideration only when the perturbative
 effects produced by the pressure of the solar radiation
 (both direct and indirect) will reach a knowledge, in their
 main spectral components, at an acceleration level of the
 order of a few 10^{-10} m/s², however a very difficult task to
 accomplish.

Returning to fundamental physics measurements, at
 the current state of the development of G4S_2.0 activ-
 ities, it is not possible to give a reliable answer on
 what the requirements of the NGPs models should be,
 for example, on the measurement of the relativistic
 Schwarzschild precession or on that of the gravitational
 redshift to obtain results comparable (or superior) to
 those reported in the literature on such tests of gravitation
 [7,8,33,34]. Meanwhile, as underlined in Sec. IVA, the
 final precision of the models must be evaluated only when
 they are completely used in the POD of the satellites for
 the reduction of the tracking data, whether laser or
 microwave. This very important aspect will be the subject
 of our future investigations, as was done in the past in the
 case of the LAGEOS and LAGEOS II geodetic satellites.
 In the case of the previous measurements on the gravi-
 tational redshift with the Galileo satellites in elliptical
 orbit, no information emerges from the literature regard-
 ing this aspect.

Of course, a general improvement in POD, thanks to
 better and more reliable models than the state of the art,
 will produce an improvement in fundamental physics
 measurements, but it is not certain that this improvement
 will be equally distributed among all the different types
 of measurements to be performed. For example, if the
 dynamical model is unable to prevent long-term effects
 in some orbital elements such as the pericenter, which
 constitutes the main observable for measuring the
 Schwarzschild precession, this will certainly impact this
 measure, but will in general be negligible in the estimation
 of the clock-bias and consequently in the measurement of
 the gravitational redshift.

1664

ACKNOWLEDGMENTS

1665 This work is part of the G4S_2.0 project, developed under the auspices of the Italian Space Agency (ASI) within
 1666 the frame of the Bando Premiale CI-COT-2018-085, under the Accordo Attuativo No. 2021-14-HH.0, with co-participation of
 1667 the Italian Institute for Astrophysics (INAF) and the Politecnico di Torino (POLITO).

1668

- 1669 [1] F. Vespe, D. Lucchesi, A. Tartaglia, G. Delle Monache, R. 1717
 1670 Peron, E. Rosciano, F. Santoli, and M. Visco, GALILEO 1718
 1671 for Science project (G4S): An opportunity to perform new 1719
 1672 measurements in fundamental physics, in *Proceedings* 1720
 1673 *of the 6th International Colloquium on Scientific and* 1721
 1674 *Fundamental Aspects of GNSS/Galileo* (European Space 1722
 1675 Agency, Valencia, Spain, 2017). 1723
- 1676 [2] F. Vespe, GALILEO for Science project (G4S): Eccentric 1724
 1677 GALILEO satellites for general relativistic investigations, 1725
 1678 in *Proceedings of the 42nd COSPAR Scientific Assembly* 1726
 1679 (COSPAR, Pasadena, 2018), Vol. 42, p. H0.5-3-18. 1727
- 1680 [3] D. Lucchesi, G. Delle Monache, R. Peron, E. Rosciano, 1728
 1681 M. L. Ruggiero, F. Santoli, A. Tartaglia, M. Visco, and F. 1729
 1682 Vespe, The Galileo for Science (G4S) project: Fundamen- 1730
 1683 tal physics and space geodesy by the orbit analysis of the 1731
 1684 Galileo satellites DORESA and MILENA, in *Proceedings* 1732
 1685 *of the EGU General Assembly Conference Abstracts*, EGU 1733
 1686 General Assembly Conference Abstracts (EGU, Vienna, 1734
 1687 2018), p. 15185. 1735
- 1688 [4] M. L. Ruggiero, A. Tartaglia, D. Lucchesi, G. Delle 1736
 1689 Monache, R. Peron, E. Rosciano, F. Santoli, F. Vespe, 1737
 1690 and M. Visco, Fully relativistic positioning for the 1738
 1691 Galileo for Science (G4S) project, in *Proceedings of the* 1739
 1692 *EGU General Assembly Conference Abstracts*, EGU 1740
 1693 General Assembly Conference Abstracts (EGU, Vienna, 1741
 1694 2018), p. 12644. 1742
- 1695 [5] F. Sapio, D. M. Lucchesi, M. Visco, S. Benedetti, E. 1743
 1696 Fiorenza, C. Lefevre, M. Lucente, C. Magnafico, R. 1744
 1697 Peron, and F. Santoli, The Galileo for Science 1745
 1698 (G4S_2.0) project: Fundamental Physics experiments with 1746
 1699 Galileo satellites DORESA and MILENA, *Nuovo Cimento* 1747
 1700 *Soc. Ital. Fis.* **45C**, 1 (2022). 1748
- 1701 [6] A. Di Marco, F. Sapio, M. Cinelli, E. Fiorenza, C. Lefevre, 1749
 1702 P. Loffredo, D. M. Lucchesi, M. Lucente, C. Magnafico, R. 1750
 1703 Peron, F. Santoli, and M. Visco, The Galileo for Science 1751
 1704 (G4S_2.0) project: Measurement of the gravitational red- 1752
 1705 shift with Galileo satellites DORESA and MILENA, 1753
 1706 *Nuovo Cimento Soc. Ital. Fis.* **45C**, 1 (2023). 1754
- 1707 [7] S. Herrmann, F. Finke, M. Lülff, O. Kichakova, D. 1755
 1708 Puetzfeld, D. Knickmann, M. List, B. Rievers, G. 1756
 1709 Giorgi, C. Günther, H. Dittus, R. Prieto-Cerdeira, F. 1757
 1710 Dilssner, F. Gonzalez, E. Schönemann, J. Ventura- 1758
 1711 Traveset, and C. Lämmerzahl, Test of the gravitational 1759
 1712 redshift with Galileo satellites in an eccentric orbit, *Phys.* 1760
 1713 *Rev. Lett.* **121**, 231102 (2018). 1761
- 1714 [8] P. Delva, N. Puchades, E. Schönemann, F. Dilssner, C. 1762
 1715 Courde, S. Bertone, F. Gonzalez, A. Hees, C. Le Poncin- 1763
 1716 Lafitte, F. Meynadier, R. Prieto-Cerdeira, B. Sohet, J. 1764
 Ventura-Traveset, and P. Wolf, Gravitational redshift test 1717
 using eccentric Galileo satellites, *Phys. Rev. Lett.* **121**, 1718
 231101 (2018). 1719
- [9] R. F. C. Vessot and M. W. Levine, A test of the equivalence 1720
 principle using a space-borne clock, *Gen. Relativ. Gravit.* 1721
10, 181 (1979). 1722
- [10] R. F. C. Vessot, M. W. Levine, E. M. Mattison, E. L. 1723
 Blomberg, T. E. Hoffman, G. U. Nystrom, B. F. Farrel, R. 1724
 Decher, P. B. Eby, C. R. Baugher, J. W. Watts, D. L. Teuber, 1725
 and F. D. Wills, Test of relativistic gravitation with a space- 1726
 borne hydrogen maser, *Phys. Rev. Lett.* **45**, 2081 (1980). 1727
- [11] V. Formichella, L. Galleani, G. Signorile, and I. Sesia, 1728
 Time–frequency analysis of the Galileo satellite clocks: 1729
 Looking for the J2 relativistic effect and other periodic 1730
 variations, *GPS Solution* **25**, 56 (2021). 1731
- [12] J. Kouba, Testing of general relativity with two Galileo 1732
 satellites in eccentric orbits, *GPS Solution* **25**, 139 (2021). 1733
- [13] A. Einstein, Die Grundlage der allgemeinen relativitäts- 1734
 theorie, *Ann. Phys.* **354**, 769 (1916), [https://onlinelibrary](https://onlinelibrary.wiley.com/doi/epdf/10.1002/andp.19163540702) 1735
[.wiley.com/doi/epdf/10.1002/andp.19163540702](https://onlinelibrary.wiley.com/doi/epdf/10.1002/andp.19163540702). 1736
- [14] C. M. Will, *Theory and Experiment in Gravitational* 1737
Physics (Cambridge University Press, Cambridge, 1738
 United Kingdom, 2018). 1739
- [15] M. Rothacher, GENESIS: GNSS/NAV science programme, 1740
 in *GSAC: Galileo Science Advisory Committee, ESA PB* 1741
NAV Workshop on CM22 (Javier Ventura Traveset, 2021). 1742
- [16] G. Beutler, E. Brockmann, W. Gurtner, U. Hugentobler, 1743
 L. Mervart, M. Rothacher, and A. Verdun, Extended orbit 1744
 modeling techniques at the CODE processing center of the 1745
 international GPS service for geodynamics (IGS): Theory 1746
 and initial results, *Manuscripta Geod.* **19**, 367 (1994). 1747
- [17] C. Rodriguez-Solano, U. Hugentobler, and P. 1748
 Steigenberger, Adjustable box-wing model for solar radi- 1749
 ation pressure impacting GPS satellites, *Adv. Space Res.* 1750
49, 1113 (2012). 1751
- [18] D. Arnold, M. Meindl, G. Beutler, R. Dach, S. Schaer, 1752
 S. Lutz, L. Prange, K. Sošnica, L. Mervart, and A. Jäggi, 1753
 CODE’s new solar radiation pressure model for GNSS 1754
 orbit determination, *J. Geodes.* **89**, 775 (2015). 1755
- [19] O. Montenbruck, P. Steigenberger, and U. Hugentobler, 1756
 Enhanced solar radiation pressure modeling for Galileo 1757
 satellites, *J. Geodes.* **89**, 283 (2015). 1758
- [20] G. Bury, K. Sošnica, R. Zajdel, and D. Strugarek, Toward 1759
 the 1-cm Galileo orbits: Challenges in modeling of 1760
 perturbing forces, *J. Geodes.* **94**, 16 (2020). 1761
- [21] F. L. Whipple and Z. Sekanina, Comet Encke–precession 1762
 of the spin axis, nongravitational motion, and sublimation, 1763
Astron. J. **84**, 1894 (1979). 1764

- 1765 [22] W. M. Smart, John Couch ADAMS and the discovery of
1766 Neptune, *Pop. Astron.* **55**, 301 (1947).
1767 [23] A. Milani, A. M. Nobili, and P. Farinella, *Non-*
1768 *Gravitational Perturbations and Satellite Geodesy* (Adam
1769 Hilger, Bristol, 1987).
1770 [24] O. Montenbruck and E. Gill, *SatelliteOrbits—Models,*
1771 *Methods and Application* (Springer, Berlin, 2005).
1772 [25] G. Beutler, *Methods of Celestial Mechanics. Vol. I:*
1773 *Physical, Mathematical, and Numerical Principles*
1774 (Springer, New York, 2005), ISBN 3-540-40749-9.
1775 [26] G. Beutler, *Methods of Celestial Mechanics. Vol. II:*
1776 *Application to Planetary System Geodynamics and Satel-*
1777 *lite Geodesy* (Springer, New York, 2005), ISBN 3-540-
1778 40750-2.
1779 [27] B. Hofmann-Wellenhof, H. Lichtenegger, and E. Wasle,
1780 *GNSS—Global Navigation Satellite Systems—GPS, GLO-*
1781 *NASS, Galileo, and more* (Springer, New York, 2008),
1782 ISBN 978-3-211-73012-6.
1783 [28] P. Teunissen and O. Montenbruck, *Springer Handbook of*
1784 *Global Navigation Satellite Systems* (Springer, Cham,
1785 2017), <https://dx.doi.org/10.1007/978-3-319-42928-1>.
1786 [29] M. R. Pearlman, J. J. Degnan, and J. M. Bosworth, The
1787 international laser ranging service, *Adv. Space Res.* **30**,
1788 135 (2002).
1789 [30] S. C. Cohen and D. E. Smith, Lageos scientific results:
1790 Introduction, *J. Geophys. Res.* **90**, 9217 (1985).
1791 [31] I. Ciufolini, D. Lucchesi, F. Vespe, and A. Mandiello,
1792 Measurement of dragging of inertial frames and gravito-
1793 magnetic field using laser-ranged satellites, *Nuovo*
1794 *Cimento Soc. Ital. Fis.* **109A**, 575 (1996).
1795 [32] I. Ciufolini and E. C. Pavlis, A confirmation of the general
1796 relativistic prediction of the Lense-Thirring effect, *Nature*
1797 (London) **431**, 958 (2004).
1798 [33] D. M. Lucchesi and R. Peron, Accurate measurement in
1799 the field of the Earth of the general-relativistic precession
1800 of the LAGEOS II pericenter and new constraints on non-
1801 Newtonian gravity, *Phys. Rev. Lett.* **105**, 231103 (2010).
1802 [34] D. M. Lucchesi and R. Peron, LAGEOS II pericenter
1803 general relativistic precession (1993-2005): Error budget
1804 and constraints in gravitational physics, *Phys. Rev. D* **89**,
1805 082002 (2014).
1806 [35] D. Lucchesi, L. Anselmo, M. Bassan, C. Pardini, R. Peron,
1807 G. Pucacco, and M. Visco, Testing the gravitational inter-
1808 action in the field of the Earth via satellite laser ranging
1809 and the Laser Ranged Satellites Experiment (LARASE),
1810 *Classical Quantum Gravity* **32**, 155012 (2015).
1811 [36] D. M. Lucchesi, L. Anselmo, M. Bassan, C. Magnafico,
1812 C. Pardini, R. Peron, G. Pucacco, and M. Visco, General
1813 relativity measurements in the field of Earth with laser-
1814 ranged satellites: State of the art and perspectives, *Universe*
1815 **5**, 141 (2019).
1816 [37] I. Ciufolini, A. Paolozzi, E. C. Pavlis, G. Sindoni, J. Ries,
1817 R. Matzner, R. Koenig, C. Paris, V. Gurzadyan, and R.
1818 Penrose, An improved test of the general relativistic effect
1819 of frame-dragging using the LARES and LAGEOS satel-
1820 lites, *Eur. Phys. J. C* **79**, 872 (2019).
1821 [38] D. Lucchesi, M. Visco, R. Peron, M. Bassan, G. Pucacco,
1822 C. Pardini, L. Anselmo, and C. Magnafico, A 1% mea-
1823 surement of the gravitomagnetic field of the Earth with
1824 laser-tracked satellites, *Universe* **6**, 139 (2020).
[39] D. Vokrouhlicky, P. Farinella, and F. Mignard, Solar
radiation pressure perturbations for Earth satellites. I:
A complete theory including penumbra transitions, *Astron.*
Astrophys. **280**, 295 (1993), [https://articles.adsabs.harvard](https://articles.adsabs.harvard.edu/pdf/1993A%26A...280..295V)
[.edu/pdf/1993A%26A...280..295V](https://articles.adsabs.harvard.edu/pdf/1993A%26A...280..295V).
[40] D. P. Rubincam, On the secular decrease in the semimajor
axis of LAGEOS's orbit, *Celest. Mech.* **26**, 361 (1982).
[41] G. Afonso, F. Barlier, F. Mignard, M. Carpino, and P.
Farinella, Orbital effects of LAGEOS seasons and eclipses,
Ann. Geophys. **7**, 501 (1989).
[42] P. Farinella, A. M. Nobili, F. Barlier, and F. Mignard,
Effects of thermal thrust on the node and inclination of
LAGEOS, *Astron. Astrophys.* **234**, 546 (1990), [https://](https://articles.adsabs.harvard.edu/pdf/1990A%26A...234..546F)
articles.adsabs.harvard.edu/pdf/1990A%26A...234..546F.
[43] R. Scharroo, K. F. Wakker, B. A. C. Ambrosius, and R.
Noomen, On the along-track acceleration of the LAGEOS
satellite, *J. Geophys. Res.* **96**, 729 (1991).
[44] V. J. Slabinski, A numerical solution for LAGEOS thermal
thrust: The rapid-spin case, *Celest. Mech. Dyn. Astron.* **66**,
131 (1996).
[45] P. Farinella and D. Vokrouhlický, Thermal force effects on
slowly rotating, spherical artificial satellites-I. Solar heat-
ing, *Planet. Space Sci.* **44**, 1551 (1996).
[46] D. P. Rubincam, D. G. Currie, and J. W. Robbins,
LAGEOS I once-per-revolution force due to solar heating,
J. Geophys. Res. **102**, 585 (1997).
[47] G. Métris, D. Vokrouhlický, J. C. Ries, and R. J. Eanes,
Nongravitational effects and the LAGEOS eccentricity
excitations, *J. Geophys. Res.* **102**, 2711 (1997).
[48] G. Métris, D. Vokrouhlický, J. C. Ries, and R. J. Eanes,
LAGEOS spin axis and non-gravitational excitations of its
orbit, *Adv. Space Res.* **23**, 721 (1999).
[49] D. M. Lucchesi, Reassessment of the error modelling of
non-gravitational perturbations on LAGEOS II and their
impact in the lense-thirring derivation-Part II, *Planet.*
Space Sci. **50**, 1067 (2002).
[50] J. I. Andrés de la Fuente, Enhanced modelling of LAGEOS
non-gravitational perturbations, Ph.D. thesis, Delft
University Press, Sieca Repro, 2007.
[51] D. P. Rubincam, P. Knocke, V. R. Taylor, and S. Blackwell,
Earth anisotropic reflection and the orbit of LAGEOS,
J. Geophys. Res. **92**, 11662 (1987).
[52] D. M. Lucchesi, The asymmetric reflectivity effect on the
LAGEOS satellites and the germanium retroreflectors,
Geophys. Res. Lett. **30**, 1957 (2003).
[53] D. M. Lucchesi, LAGEOS satellites germanium cube-
corner-retroreflectors and the asymmetric reflectivity
effect, *Celest. Mech. Dyn. Astron.* **88**, 269 (2004).
[54] H. P. Robertson, Dynamical effects of radiation in the solar
system, *Mon. Not. R. Astron. Soc.* **97**, 423 (1937).
[55] I. I. Shapiro, The prediction of satellite orbits, in *Dynamics*
of Satellites / Dynamique des Satellites, edited by M. Roy
(Springer Berlin Heidelberg, Berlin, Heidelberg, 1963),
pp. 257–312.
[56] R. R. Allan, Resonance effects due to the longitude
dependence of the gravitational field of a rotating primary,
Planet. Space Sci. **15**, 53 (1967).
[57] D. Vokrouhlicky, P. Farinella, and F. Mignard, Solar
radiation pressure perturbations for Earth satellites. III.
Global atmospheric phenomena and the Albedo effect,

- 1885 Astron. Astrophys. **290**, 324 (1994), [https://articles.adsabs](https://articles.adsabs.harvard.edu/pdf/1994A%26A...290..324V)
 1886 [.harvard.edu/pdf/1994A%26A...290..324V](https://articles.adsabs.harvard.edu/pdf/1994A%26A...290..324V).
- 1887 [58] L. Sehnal, Effects of the terrestrial infrared radiation
 1888 pressure on the motion of an artificial satellite, *Celest.*
 1889 *Mech.* **25**, 169 (1981).
- 1890 [59] V. R. Taylor and L. L. Stowe, Reflectance characteristics of
 1891 uniform Earth and cloud surfaces derived from NIMBUS-7
 1892 ERB, *J. Geogr. Res.* **89**, 4987 (1984).
- 1893 [60] L. Anselmo, P. Farinella, A. Milani, and A. M. Nobili,
 1894 Effects of the Earth-reflected sunlight on the orbit of the
 1895 LAGEOS satellite, *Astron. Astrophys.* **117**, 3 (1983),
 1896 [https://articles.adsabs.harvard.edu/pdf/1983A%26A...117...](https://articles.adsabs.harvard.edu/pdf/1983A%26A...117...3A)
 1897 [...3A](https://articles.adsabs.harvard.edu/pdf/1983A%26A...117...3A).
- 1898 [61] D. P. Rubincam and N. S. Weiss, Earth Albedo and the
 1899 orbit of LAGEOS, *Celest. Mech.* **38**, 233 (1986).
- 1900 [62] F. Barlier, M. Carpino, P. Farinella, F. Mignard, A. Milani,
 1901 and A. M. Nobili, Non-gravitational perturbations on
 1902 the semimajor axis of LAGEOS, *Ann. Geophys.* **4**, 193
 1903 (1986).
- 1904 [63] D. Lucchesi and P. Farinella, Optical properties of the
 1905 Earth's surface and long-term perturbations of LAGEOS's
 1906 semimajor axis, *J. Geogr. Res.* **97**, 7121 (1992).
- 1907 [64] D. M. Lucchesi, Reassessment of the error modelling of
 1908 non-gravitational perturbations on LAGEOS II and their
 1909 impact in the Lense-Thirring determination. Part I, *Planet.*
 1910 *Space Sci.* **49**, 447 (2001).
- 1911 [65] U. Hugentobler, C. J. Rodriguez Solano, P. Steigenberger,
 1912 R. Dach, and S. Lutz, Impact of Albedo modeling
 1913 on GNSS satellite orbits and geodetic time series, in
 1914 *Proceedings of the AGU Fall Meeting Abstracts* (AGU,
 1915 San Francisco, 2009), Vol. 2009, pp. G11C–0654.
- 1916 [66] C. J. Rodriguez-Solano, Impact of Albedo modelling on
 1917 GPS orbits, Master Thesis, Ph.D. thesis, TUM, Munchen,
 1918 2009.
- 1919 [67] B. A. Wielicki, B. R. Barkstrom, E. F. Harrison, Robert B.
 1920 Lee III, G. L. Smith, and J. E. Cooper, Clouds and the
 1921 Earth's radiant energy system (CERES): An Earth observ-
 1922 ing system experiment, *Bull. Am. Meteorol. Soc.* **77**, 853
 1923 (1996).
- 1924 [68] D. P. Rubincam, Atmospheric drag as the cause of the
 1925 secular decrease in the semimajor axis of LAGEOS's orbit,
 1926 *Geophys. Res. Lett.* **7**, 468 (1980).
- 1927 [69] J. Afonso, F. Barlier, C. Berger, and F. Mignard, The effect
 1928 of atmospheric braking and electric drag on the trajectory
 1929 of the LAGEOS satellite, *Acad. Sci. Paris C. R. Ser. B* **290**,
 1930 445 (1980).
- 1931 [70] G. Afonso, F. Barlier, C. Berger, F. Mignard, and J. J.
 1932 Walch, Reassessment of the charge and neutral drag of
 1933 LAGEOS and its geophysical implications, *J. Geophys.*
 1934 *Res.* **90**, 9381 (1985).
- 1935 [71] C. Pardini, L. Anselmo, D. M. Lucchesi, and R. Peron, On
 1936 the secular decay of the LARES semi-major axis, *Acta*
 1937 *Astronaut.* **140**, 469 (2017).
- 1938 [72] B. King-Hele, Theory of satellite orbits in an atmosphere,
 1939 *Q. J. R. Meteorol. Soc.* **90**, 503 (1964).
- 1940 [73] D. P. Rubincam, Drag on the LAGEOS satellite,
 1941 *J. Geophys. Res.* **95**, 4881 (1990).
- 1942 [74] D. Vokrouhlický and P. Farinella, Thermal force effects on
 1943 slowly rotating, spherical artificial satellites—II. Earth
 1944 infrared heating, *Planet. Space Sci.* **45**, 419 (1997).
- [75] Y. Vigue, P. A. M. Abusali, and B. E. Schutz, Thermal
 force modeling for global positioning system using the
 finite element method, *J. Spacecraft Rockets* **31**, 855
 (1994).
- [76] H. F. Fliegel and T. E. Gallini, Solar force modeling of
 block IIR global positioning system satellites, *J. Spacecraft*
Rockets **33**, 863 (1996).
- [77] W. Marquis and C. Krier, Examination of the GPS block
 IIR solar pressure model, in *Proceedings of the 13th*
International Technical Meeting of the Satellite
Division of the Institute of Navigation (ION GPS 2000),
Salt Lake City, UT (2000), pp. 407–415.
- [78] J. Duha, G. B. Afonso, and L. D. D. Ferreira, Thermal re-
 emission effects on GPS satellites, *J. Geodes.* **80**, 665
 (2006).
- [79] The next generation of *Galileo* satellites will also be
 equipped with movable antennas for inter-satellite link.
- [80] P. Steigenberger, S. Thielert, and O. Montenbruck, GNSS
 satellite transmit power and its impact on orbit determi-
 nation, *J. Geodes.* **92**, 609 (2018).
- [81] Y. E. Bar-Sever, New and improved solar radiation
 pressure models for GPS satellites based on flight
 data, JPL-CA, Jet Propulsion Laboratory, California
 Institute of Technology Technical Report No. TR 80-
 4193, 1997.
- [82] T. A. Springer, G. Beutler, and M. Rothacher, A new solar
 radiation pressure model for GPS, *Adv. Space Res.* **23**, 673
 (1999).
- [83] Y. Bar-Sever and D. Kuang, New empirically derived solar
 radiation pressure model for global positioning system
 satellites, *Interplanet. Network Prog. Rep.* **42–159**, 1
 (2004), [https://ipnpr.jpl.nasa.gov/progress_report/42-159/](https://ipnpr.jpl.nasa.gov/progress_report/42-159/159I.pdf)
[159I.pdf](https://ipnpr.jpl.nasa.gov/progress_report/42-159/159I.pdf).
- [84] Y. Bar-Sever and D. Kuang, New empirically derived solar
 radiation pressure model for global positioning system
 satellites during eclipse seasons, *Interplanet. Network*
Prog. Rep. **42–160**, 1 (2005), [https://ipnpr.jpl.nasa.gov/](https://ipnpr.jpl.nasa.gov/progress_report/42-160/160I.pdf)
[progress_report/42-160/160I.pdf](https://ipnpr.jpl.nasa.gov/progress_report/42-160/160I.pdf).
- [85] B. Fritsche, M. Ivanov, A. Kashkovsky *et al.*, Radiation
 pressure forces on complex spacecraft, HTG, Germany
 and ITAM, Russian, ESOC Contract 11908/96/D/IM,
 Technical Report TN, 1998.
- [86] H. Klinkrad and B. Fritsche, Orbit and attitude perturba-
 tions due to aerodynamics and radiation pressure, ESTEC
 Technical Report TN, 1998.
- [87] H. Klinkrad, C. Koeck, and P. Renard, Precise satellite
 skin-force modelling by means of Monte-Carlo ray tracing,
ESA J. **14**, 409 (1990).
- [88] H. Klinkrad, C. Koeck, and P. Renard, Key features of a
 satellite skin force modelling technique by means of
 Monte-Carlo ray tracing, *Adv. Space Res.* **11**, 147 (1991).
- [89] M. Ziebart, High precision analytical solar radiation
 pressure modelling for GNSS spacecraft, Ph.D. Thesis,
 University of East London, 2001.
- [90] M. Ziebart and P. Dare, Analytical solar radiation pressure
 modelling for GLONASS using a pixel array, *J. Geodes.*
75, 587 (2001).
- [91] B. Tan, Y. Yuan, B. Zhang, H. Z. Hsu, and J. Ou, A new
 analytical solar radiation pressure model for current
 BeiDou satellites: IGGBSPM, *Sci. Rep.* **6**, 32967 (2016).

- 2005 [92] O. Montenbruck, P. Steigenberger, and F. Darugna, Semi-
 2006 analytical solar radiation pressure modeling for QZS-1
 2007 orbit-normal and yaw-steering attitude, *Adv. Space Res.*
 2008 **59**, 2088 (2017).
- 2009 [93] Z. Li, Space vehicle radiation pressure modelling: A
 2010 demonstration on Galileo satellites in GNSS, Ph.D. thesis,
 2011 Department of Civil, Environmental and Geomagnetic
 2012 Engineering, University of College London, 2018.
- 2013 [94] Z. Li, M. Ziebart, S. Bhattarai, D. Harrison, and S. Grey,
 2014 Fast solar radiation pressure modelling with ray tracing
 2015 and multiple reflections, *Adv. Space Res.* **61**, 2352 (2018).
- 2016 [95] G. Bury, R. Zajdel, and K. Sošnica, Accounting for
 2017 perturbing forces acting on Galileo using a box-wing
 2018 model, *GPS Solut.* **23**, 74 (2019).
- 2019 [96] M. Ziebart, Analytical SRP model for GLONASS: Initial
 2020 results, Applied Geodesy Research Unit, School of Sur-
 2021 veying, University of East London Technical Report, 1998.
- 2022 [97] M. Ziebart, Generalized analytical solar radiation pressure
 2023 modeling algorithm for spacecraft of complex shape,
 2024 *J. Spacecraft Rockets* **41**, 840 (2004).
- 2025 [98] B. Rievers, C. Lämmerzahl, M. List, S. Bremer, and H.
 2026 Dittus, New powerful thermal modelling for high-precision
 2027 gravity missions with application to Pioneer 10/11, *New J.*
 2028 *Phys.* **11**, 113032 (2009).
- 2029 [99] F. Darugna, Solar radiation pressure modeling for the
 2030 QZS-1 satellite, Ph.D. thesis, Dipartimento di Ingegneria
 2031 Industriale e Dipartimento di Fisica e Astronomia,
 2032 Università degli Studi di Padova, Italy, 2017.
- 2033 [100] F. Finke, Test of general relativity with GALILEO satel-
 2034 lites, Ph.D. thesis, University of Bremen, 2023.
- 2035 [101] P. Delva, N. Puchades, E. Schönemann, F. Dilssner, C.
 2036 Courde, S. Bertone, F. Gonzalez, A. Hees, C. Le Poncin-
 2037 Lafitte, F. Meynadier, R. Prieto-Cerdeira, B. Sohet, J.
 2038 Ventura-Traveset, and P. Wolf, Gravitational redshift test
 2039 using eccentric Galileo satellites: Supplemental material,
 2040 *Phys. Rev. Lett.* **121**, 231101 (2018).
- 2041 [102] F. Gini, GOCE precise non-gravitational force modeling
 2042 for POD applications, Ph.D. thesis, CISAS, Padova, Italy,
 2043 2014.
- 2044 [103] M. R. Drinkwater, R. Floberghagen, R. Haagmans, D. Muzi,
 2045 and A. Popescu, VII: Closing session: GOCE: ESA's first
 2046 Earth explorer core mission, *Space Sci. Rev.* **108**, 419 (2003).
- 2047 [104] M. Meindl, G. Beutler, D. Thaller, R. Dach, and A. Jäggi,
 2048 Geocenter coordinates estimated from GNSS data as
 2049 viewed by perturbation theory, *Adv. Space Res.* **51**,
 2050 1047 (2013).
- 2051 [105] K. Sošnica, G. Bury, R. Zajdel, D. Strugarek, M.
 2052 Drożdżewski, and K. Kazmierski, Estimating global geo-
 2053 detic parameters using SLR observations to Galileo,
 2054 GLONASS, BeiDou, GPS, and QZSS, *Earth Planets Space*
 2055 **71**, 20 (2019).
- 2056 [106] H. F. Fliegel, T. E. Gallini, and E. R. Swift, Global posi-
 2057 tioning system radiation force model for geodetic appli-
 2058 cations, *J. Geophys. Res.* **97**, 559 (1992).
- 2059 [107] A. Jäggi, U. Hugentobler, and G. Beutler, Pseudo-stochastic
 2060 orbit modeling techniques for low-Earth orbiters, *J. Geodes.*
 2061 **80**, 47 (2006).
- 2062 [108] G. Beutler, A. Jäggi, U. Hugentobler, and L. Mervart,
 2063 Efficient satellite orbit modelling using pseudo-stochastic
 2064 parameters, *J. Geodes.* **80**, 353 (2006).
- [109] Galileo Metadata, <https://www.gsc-europa.eu/support-to-developers/galileo-satellite-metadata#6>. 2065
- [110] R. C. Willson, The total solar irradiance record and its 2066
 continuity, in *Proceedings of AGU Fall Meeting Abstracts*
 (AGU, San Francisco, 2007), Vol. 2007, p. GC42A-03. 2067
- [111] Recall that the rotation of the Sun, since it varies with 2068
 varying latitude, is of a differential type. The average
 rotation period is about 28-Earth days. 2069
- [112] G. de Toma, O. R. White, G. A. Chapman, and S. R. 2070
 Walton, Solar irradiance variability: Progress in measure-
 ment and empirical analysis, *Adv. Space Res.* **34**, 237 2071
 (2004). 2072
- [113] S. K. Solanki and Y. C. Unruh, Solar irradiance variability, 2073
Astron. Nachr. **334**, 145 (2013). 2074
- [114] S. Lutz, M. Meindl, P. Steigenberger, G. Beutler, K. 2075
 Sošnica, S. Schaer, R. Dach, D. Arnold, D. Thaller, and
 A. Jäggi, Impact of the arc length on GNSS analysis 2076
 results, *J. Geodes.* **90**, 365 (2016). 2077
- [115] J. I. Andrés, R. Noomen, G. Bianco, D. G. Currie, and T. 2078
 Otsubo, Spin axis behavior of the LAGEOS satellites,
J. Geophys. Res. **109**, 2994 (2004). 2079
- [116] M. Visco and D. M. Lucchesi, Review and critical analysis 2080
 of mass and moments of inertia of the LAGEOS and
 LAGEOS II satellites for the LARASE program, *Adv. Space 2081
 Res.* **57**, 1928 (2016). 2082
- [117] M. Visco and D. M. Lucchesi, Comprehensive model for 2083
 the spin evolution of the LAGEOS and LARES satellites,
Phys. Rev. D **98**, 044034 (2018). 2084
- [118] M. Cheng, B. D. Tapley, and J. C. Ries, Deceleration in the 2085
 Earth's oblateness, *J. Geophys. Res.* **118**, 740 (2013). 2086
- [119] B. D. Tapley and C. Reigber, The GRACE mission: Status 2087
 and future plans, in *AGU Fall Meeting Abstracts* (AGU,
 San Francisco, 2001), p. G41C-02. 2088
- [120] G. Petit and B. Luzum, *IERS Conventions (2010)*, 2089
 IERS Technical Note 36 (IERS, Verlag des Bundesamts
 für Kartographie und Geodäsie, Frankfurt am Main, 2090
 2010). 2091
- [121] D. M. Lucchesi, I. Ciufolini, J. I. Andrés, E. C. Pavlis, R. 2092
 Peron, R. Noomen, and D. G. Currie, LAGEOS II perigee
 rate and eccentricity vector excitations residuals and the 2093
 Yarkovsky-Schach effect, *Planet. Space Sci.* **52**, 699 2094
 (2004). 2095
- [122] Z. Li and M. Ziebart, Uncertainty analysis on direct solar 2096
 radiation pressure modelling for GPS IIR and Galileo FOC
 satellites, *Adv. Space Res.* **66**, 963 (2020). 2097
- [123] F. Sapia *et al.*, following article, Fundamental physics 2098
 measurements with Galileo FOC satellites and the Galileo
 for Science project. Part II: A box wing for modeling direct 2099
 solar radiation pressure and preliminaries orbit determi-
 nations, *Phys. Rev. D*, **109**, DG13638 (2024). 2100
- [124] This allows a better comparison with the intrinsic charac- 2101
 teristics of an accelerometer to be used for the direct
 measurement of the main nongravitational accelerations. 2102
 These direct measurements must be at least competitive 2103
 with the indirect measurements provided by the models 2104
 themselves. In fact, an advantage of an accelerometer 2105
 compared to the models is provided by the process of 2106
 integration of the measures, which translates into a more 2107
 precise determination of the amplitude of the various 2108
 disturbing effects. 2109
 2110
 2111
 2112
 2113
 2114
 2115
 2116
 2117
 2118
 2119
 2120
 2121
 2122
 2123
 2124

- 2125 [125] The L-band antenna is used for broadcasting the navigation 2137
2126 message down to on ground receivers. SAR are UHF 2138
2127 antennas designed to collect emergency messages from 2139
2128 ships in evident danger and to be transmitted to search 2140
2129 and rescue authorities. SAR antennas contribute to the 2141
2130 international COSPAS-SARSAT system. The C-band an- 2142
2131 tenna receives mission data and navigation corrections 2143
2132 from uplink stations on the ground. 2144
2133 [126] www.sketchup.com. 2145
2134 [127] www.solidworks.com. 2146
2135 [128] Biovia, *Dassault systèmes, solidworks, version 2017* 2147
2136 (Dassault Systèmes, San Diego, CA, 2017). 2148
- [129] COMSOL Multiphysics® Reference Manual, Version 5.5, 2137
COMSOL Multiphysics [Burlington, MA] (1998–2019). 2138
[130] COMSOL Heat Transfer Module® User’S Guide, 2139
Version 5.4, COMSOL Multiphysics, [Burlington, MA] 2140
(1998–2018). 2141
[131] <https://www.mathworks.com>. 2142
[132] D. E. Pavlis *et al.*, *GEODYN II Operations Manual* (NASA 2143
GSFC, Greenbelt, 1998). 2144
[133] D. M. Lucchesi and G. Balmino, The LAGEOS satellites 2145
orbital residuals determination and the Lense 2146
Thirring effect measurement, *Planet. Space Sci.* **54**, 581 2147
(2006). **Q1** 2148
2149